Contributions to Mineralogy and Petrology (2019) 174:23
https://doi.org/10.1007/s00410-019-1557-7

ORIGINAL PAPER

Reconsideration of Neo-Tethys evolution constrained from the nature of the Dazhuqu ophiolitic mantle, southern Tibet

Tong Liu[1,2] · Fu-Yuan Wu[1,2,3] · Chuan-Zhou Liu[1,3,4] · Chang Zhang[1] · Wen-Bin Ji[1] · Yang Xu[1]

Received: 18 October 2018 / Accepted: 22 February 2019 / Published online: 4 March 2019

Abstract

The nature (i.e., sub-oceanic, sub-arc or sub-continental) of ophiolitic mantle peridotites from the eastern Neo-Tethyan domain in southern Tibet has been hotly debated. This uncertainty limits our understanding of the history and evolution of the eastern Neo-Tethys Ocean. Here we present petrological, geochemical and Re–Os isotopic data for the mantle peridotites from the Dazhuqu ophiolite in the central segment of the Yarlung Zangbo suture zone, southern Tibet. Samples collected include both spinel lherzolites and spinel harzburgites. The lherzolites have spinel Cr# [Cr/(Cr + Al), ~ 0.3–0.4] comparable to those of typical abyssal peridotites. In contrast, the harzburgites have spinel Cr# (~ 0.3–0.7) overlapping with the ranges of both abyssal and fore-arc peridotites; two samples have spinel Cr# higher than 0.6, which is probably ascribed to intense melt–rock interactions. Clinopyroxene trace element modeling indicates that the Dazhuqu mantle peridotites have experienced 0–6% garnet-facies melting followed by 10–18% melting in the spinel stability field. This is similar to the degree of garnet-facies melting inferred for many abyssal peridotites and implies deep initial melting (> 85 km), which distinguishes the Dazhuqu mantle peridotites from fore-arc peridotites (commonly < 80 km in origin). The Dazhuqu peridotites have unradiogenic $^{187}Os/^{188}Os$ of 0.11836–0.12922, which are commonly lower than the recommended value of primitive upper mantle (PUM). All but one samples yield relatively younger Re depletion ages (T_{RD} = 0.06–0.81 Ga) with respect to the only one sample having an older T_{RD} age of 1.66 Ga. Re–Os isotopes and highly siderophile element (HSE) compositions of the Dazhuqu peridotites are similar to those of abyssal peridotites and the Oman southern massifs but are distinct from non-cratonic sub-continental lithospheric mantle (SCLM) xenoliths and sub-arc mantle. We emphasize the similarity between the Dazhuqu and Oman ophiolites, both representing Neo-Tethyan oceanic lithosphere and implying ridge–trench collision.

Keywords Neo-Tethys Ocean · Sub-oceanic mantle · Re–Os isotope · Mantle peridotite · Dazhuqu ophiolite · Yarlung Zangbo suture zone

Introduction

A Wilson cycle describes the tectonic evolution of ocean basins from continental rifting, through ocean opening, subduction to closure (Wilson 1968). Consequently, much of the history of a disappeared ocean is "hidden" in ophiolites, which are regarded as fragments of oceanic lithosphere emplaced onto continents (Gass 1968; Moores and Vine 1971). In the past four decades, however, numerous studies have demonstrated, based on geochemical fingerprinting, that a significant proportion of ophiolites worldwide were generated at subduction zones rather than at mid-ocean ridges (Alabaster et al. 1982; Miyashiro 1973; Pearce et al. 1984; Pearce and Robinson 2010; Whattam and Stern 2011). The former has been classified as supra-subduction zone (SSZ) ophiolites, whereas the latter has been termed

Communicated by Othmar Müntener.

Electronic supplementary material The online version of this article (https://doi.org/10.1007/s00410-019-1557-7) contains supplementary material, which is available to authorized users.

✉ Tong Liu
liutong@mail.iggcas.ac.cn

[1] State Key Laboratory of Lithospheric Evolution, Institute of Geology and Geophysics, Chinese Academy of Sciences, Beijing 100029, China

[2] Institutions of Earth Science, Chinese Academy of Sciences, Beijing 100029, China

[3] University of Chinese Academy of Sciences, Beijing 100049, China

[4] CAS Center for Excellence in Tibetan Plateau Earth Sciences, Beijing 100101, China

mid-ocean ridge (MOR) ophiolites (Alabaster et al. 1982). A SSZ ophiolite is newly born as a consequence of oceanic crustal accretion mostly in a fore-arc basin and may mark major subduction initiation processes (Dilek and Furnes 2011; Whattam and Stern 2011). Based on this hypothesis, peridotites within certain ophiolites are often interpreted as juvenile fore-arc mantle (sub-arc mantle), rather than as abyssal peridotites beneath MOR (sub-oceanic mantle). On the other hand, ancient (> 1.0 Ga) osmium isotope signatures indicate in one aspect a sub-continental lithospheric mantle (SCLM) affinity for some ophiolitic peridotites, e.g., the Alpine–Apennine ophiolites [ages were recalculated from the osmium data reported by Alard et al. (2005), Snow et al. (2000) and van Acken et al. (2008)]. An extensively accepted interpretation is that such SCLM-type peridotites were exhumed and emplaced close to the rifted continental margins and ocean–continent transition (OCT) settings (e.g., McCarthy and Müntener 2015; Müntener and Manatschal 2006; Rampone et al. 1998; Tribuzio et al. 2004). These observations diminish the direct linkage between ophiolites and disappeared oceanic lithospheres.

The Neo-Tethys Ocean is an ocean that existed between the continents of Gondwana and Eurasia during much of the Mesozoic (Gehrels et al. 2011; Metcalfe 2006; Sengor and Natalin 1996). The eastern part of Neo-Tethys Ocean closed along the Yarlung Zangbo suture zone (YZSZ) in southern Tibet (Dewey et al. 1988; Pan et al. 2012; Yin and Harrison 2000; Zhu et al. 2013). The best geologic record of this ancient ocean observed to date is the E–W trending Yarlung Zangbo ophiolites, which have been regarded as peculiar fragments of oceanic lithosphere emplaced onto the Indian plate (Girardeau et al. 1985a, b; Nicolas et al. 1981). Recent studies, however, have argued that the Yarlung Zangbo ophiolites formed in a fore-arc (Dai et al. 2011, 2013; Xia et al. 2003; Xiong et al. 2016, 2017) or back-arc basin (Hébert et al. 2012 and references therein) and could not represent the "true" Neo-Tethyan oceanic lithosphere. A bone of contention is the nature of the mantle peridotites within these ophiolites. Geochemical observations revealed that some mantle massifs along the YZSZ experienced high degrees of partial melting and displayed U-shaped whole-rock rare earth element (REE) patterns (Dai et al. 2011, 2013; Xia et al. 2003; Xiong et al. 2017; Zhou et al. 2005). The two features were ascribed to an interaction between depleted mantle peridotites and boninitic melts (Dai et al. 2011, 2013; Zhou et al. 2005) and hence support a fore-arc tectonic setting. However, these arguments are confusing because abyssal peridotites at modern ocean ridges also sometimes show U-shaped or spoon-like whole-rock REE patterns (e.g., Day et al. 2017). On the other hand, Gong et al. (2016) and Griffin et al. (2016) argued that ancient mantle signatures in the Yarlung Zangbo ophiolites, along with the relatively high Na but low Nd contents in clinopyroxenes, provide evidence for a SCLM affinity, as is the case for the Alpine–Apennine ophiolites (Alard et al. 2005; Müntener et al. 2010; Snow et al. 2000; van Acken et al. 2008). The mantle massif examined in previous studies (i.e., the Purang mantle peridotites from the western YZSZ; Gong et al. 2016), however, displays Os isotopic ratios that are consistent with those of certain abyssal peridotites (e.g., Day et al. 2017; Harvey et al. 2006; Lassiter et al. 2014; Liu et al. 2008). These complex results underscore the need for a systematic Re–Os study of the Yarlung Zangbo ophiolitic mantle. Definition of the nature (sub-oceanic, sub-continental or sub-arc) of these mantle rocks, based on systematic observations of their petrological and chemical features, is absolutely critical to decipher the origin of the Yarlung Zangbo ophiolites and hence to reconstruct the history of the Neo-Tethys Ocean.

In this study, we present mineral, petrological and geochemical compositions of mantle peridotites collected from the Dazhuqu ophiolite in the central segment of the YZSZ. These results suggest that the Dazhuqu mantle peridotites are of sub-oceanic affinity, rather than representing SCLM or sub-arc mantle. They are suitable for establishing the link between the Yarlung Zangbo ophiolites and the Neo-Tethyan oceanic lithosphere, and thus advancing our understanding of the evolutionary history of the Neo-Tethys Ocean.

Geological framework and sample description

Geological framework

The Tibetan plateau is a collage of several tectonostratigraphic terranes (Fig. 1a), which are separated by different E–W trending sutures (Dewey et al. 1988; Pan et al. 2012; Sengor and Natalin 1996; Yin and Harrison 2000; Zhu et al. 2013). The YZSZ is the southernmost suture (Fig. 1a, b) and has been regarded as the site where the Neo-Tethys Ocean closed (Yin and Harrison 2000; Zhu et al. 2013). Ophiolites in the YZSZ extend discontinuously about 2000 km from the Nanga Parbat syntaxis in the west to the Namche Barwa syntaxis in the east (Hébert et al. 2012). Traditionally, the Yarlung Zangbo ophiolites have been divided into three segments from west to east. Ophiolites in the central segment are also termed the Xigaze ophiolite, including ophiolitic massifs in Ngamring, Jiding, Luqu and Dazhuqu (Bao et al. 2013). They were sandwiched between the Xigaze fore-arc basin (XFB) sedimentary rocks to the north and the Triassic–Cretaceous accretionary mélanges to the south (Fig. 1b). The base of the XFB sediments is the Chongdui Formation, which is a tuffaceous chert section with interbedded tuff layers of 119–113 Ma (Wang et al. 2017).

Overall, the Xigaze ophiolite has lithological assemblages that are quite distinct from the ideal "Penrose-type" ophiolite

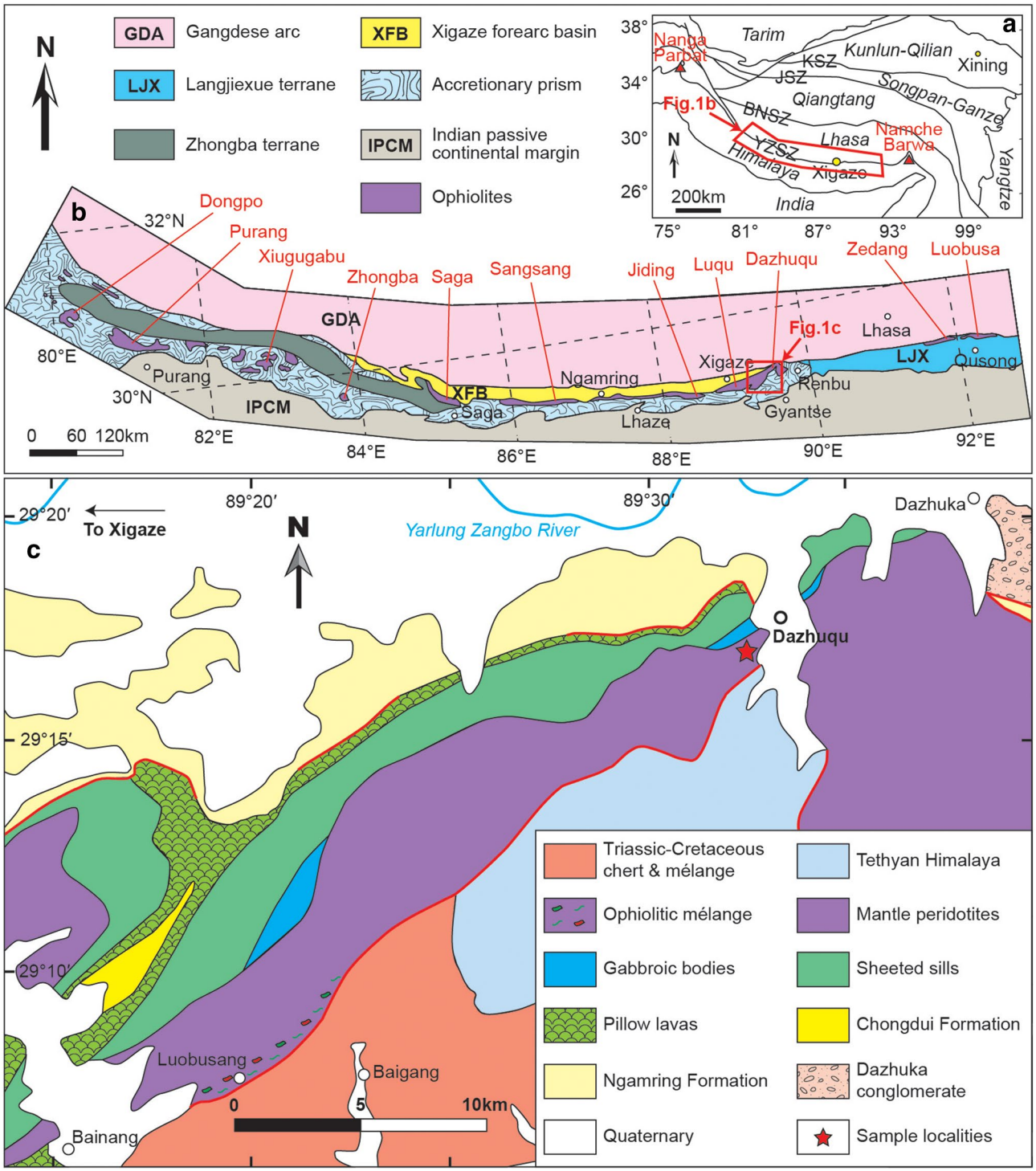

Fig. 1 **a** Simplified geological map of the Tibetan Plateau showing the major terranes and sutures; modified after Wu et al. (2008). *KSZ* Kunlun suture zone, *JSZ* Jinsha suture zone, *BNSZ* Bangong–Nujiang suture zone, *YZSZ* Yarlung Zangbo suture zone. **b** Geological map of southern Tibet illustrating the distribution of the Yarlung Zangbo ophiolites; modified after Dai et al. (2011). **c** Simplified geological map of the Dazhuqu ophiolite, modified after Wang et al. (1987)

sequence (Nicolas et al. 1981). Mantle peridotites from the Dazhuqu (also termed Lianxiang or West Dazhuka) massif in the eastern part of the Xigaze ophiolite have a maximum thickness of about 4.5 km and are overlain by ~ 3 km thick crustal rocks (Fig. 1c), including gabbros, diabases and basalts (Girardeau et al. 1985b). Geochronological studies

of the crustal rocks indicate that the Dazhuqu ophiolite was generated during 124–128 Ma (Dai et al. 2013; Liu et al. 2016; Malpas et al. 2003), which is coeval with the age of radiolarian cherts overlying the ophiolite (Upper Barremian; Ziabrev et al. 2003). Gabbros from the Dazhuqu ophiolite occur as layered intrusions of hundreds of meters in thickness or as meter-scale veins intruding into the mantle section. Both uppermost mantle and gabbro sections are cross-cut ubiquitously by diabase dikes or sills. Diabases proportionally increase upwards and transfer gradationally into a sheeted sill complex, with a strike parallel to the main foliation of the peridotites and to the major lithostratigraphic unit boundaries (Girardeau et al. 1985a, b). The sheeted sill complex is overlain by pillow and massive basaltic lavas, which in turn are commonly in thrust contact with the XFB sedimentary rocks. These geological features have been used to suggest that the Dazhuqu ophiolite was generated at a slow- to ultraslow-spreading MOR setting (Girardeau et al. 1985a, b; Nicolas et al. 1981; Liu et al. 2016; Wang et al. 1987; Wu et al. 2014).

Sample description

Mantle peridotites from the Dazhuqu ophiolite has commonly been subjected to intense alteration, but remarkably fresh peridotites occur as domes within the serpentinized peridotites (Fig. 2a, b). They mainly consist of harzburgites with volumetrically subordinate lherzolites (Fig. 2c). The field relationship between harzburgites and lherzolites is, however, obscure. Occasionally, irregular dunite patches (1–10 m) occur within the harzburgites (Fig. 2d). Some of the fresh peridotites commonly display clear primary high-temperature foliations. Occasionally, the mantle peridotites are cross-cut by different pyroxenite veins, including clinopyroxenites, orthopyroxenites and websterites (Fig. 2e). Northwards, the uppermost part of the mantle section is commonly intruded by diabase, rodingite and gabbroic dikes or sills (Fig. 2f).

Thirty-three peridotites from the Dazhuqu massif have been studied (GPS: N 29°16.41′, E 89°31.66′). Among them, 21 samples are spinel harzburgites, which have clinopyroxene modal compositions varying from 0.7 to 4.9%, and the rest are spinel lherzolites with clinopyroxene modal compositions of 5.1–7.3% (Table 1; modal composition estimates are based on systematic petrographic observations, and on combined calculations using whole-rock and mineral major element compositions). Spinel harzburgites are composed of fresh olivine, orthopyroxene, clinopyroxene and spinel. Three out of the 21 harzburgites show a protogranular texture, in which olivine and orthopyroxene display curvilinear and polygonal shapes and are also locally recrystallized and show triple junctions (Fig. 3a). 18 of the Dazhuqu harzburgite samples display a porphyroclastic texture, in which both olivine and orthopyroxene porphyroclasts are surrounded by fine-grained neoblasts (Fig. 3b). Thin (< 10 μm) exsolution lamellae of clinopyroxenes are widely developed in orthopyroxene porphyroclasts (Fig. 3b), indicating Ca saturation over the major cooling path. This is consistent with a closure temperature of 867–1139 °C based on the calculation using the Ca-in-orthopyroxene geothermometer proposed by Brey and Köhler (1990) (at a given pressure of 15 kbar).

Clinopyroxenes from the Dazhuqu harzburgites commonly occur as small grains (0.1–0.2 mm), while those from lherzolite samples developed into porphyroclasts with a grain size of ~ 2 mm (Fig. 3c). Brownish spinels are ubiquitous in both the Dazhuqu harzburgites and lherzolites and commonly show a holly-leaf shape (Fig. 3d). They occasionally occur as inclusions within orthopyroxenes and olivines. The lherzolites and harzburgites show different sulfide petrographic features, with a few (< 1%) subhedral sulfides (mainly pentlandite) only occur in the former that are rare in the latter (Fig. 3e, f).

Analytical methods

Fresh Dazhuqu peridotite samples were cut to make thin-sections for petrographic observations and mineral major and trace element analyses. The residual samples were then crushed to powders with sizes of ~ 200 mesh for whole-rock major element, highly siderophile element (HSE) and Re–Os isotope measurements. All analyses conducted in this study were done at the Institute of Geology and Geophysics, Chinese Academy of Sciences (IGGCAS) in Beijing, China.

Whole-rock and mineral major element measurements

0.5 g sample powders were precisely weighted and then mixed with 5 g $Li_2B_4O_7$ to make fused glass discs for whole-rock major element analysis using an AXIOS Minerals X-ray fluorescence (XRF) spectrometer. Loss on ignition (LOI) was determined by the measurement of the relative weight loss of 0.5 g sample powder after heating in an oven at ~ 1000 °C for 1.5 h. The 95% confidence limits for XRF analysis are ± 0.04% to ± 0.05% for SiO_2 and Al_2O_3, ± 0.01% to ± 0.02% for Fe_2O_3, MgO, Na_2O and K_2O and < ± 0.01% for TiO_2, MnO, CaO and P_2O_5, respectively, according to triplicate measurements of the USGS standard GSR-1 in the lab.

Major element compositions of minerals were determined by electron probe micro-analysis (EPMA) using a JEOL JXA8100 instrument. During analysis, quantitative measurement was carried out using wavelength-dispersive spectrometers (WDS) with an accelerating voltage of 15 kV and a beam current of 20 nA. The peak and

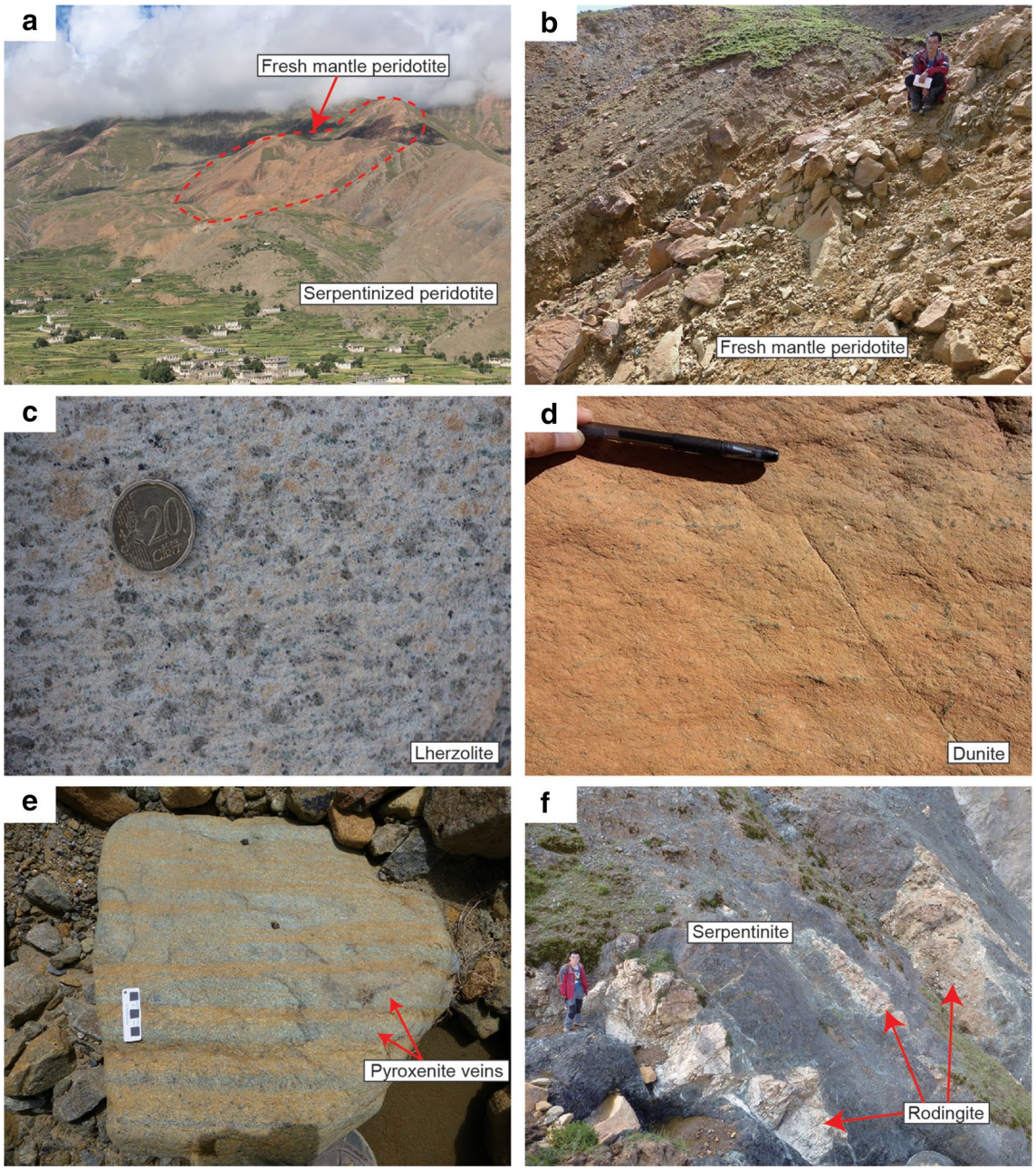

Fig. 2 Field photos of the Dazhuqu mantle peridotites. **a** Fresh mantle peridotites having a dome-like shape included by serpentinized peridotites. **b** Outcrops of fresh Dazhuqu mantle peridotites. **c** Dazhuqu lherzolites. **d** Dunites. **e** Fresh Dazhuqu mantle peridotites cross-cut by pyroxenite veins. **f** Intensely serpentinized peridotites from Dazhuqu intruded by rodingite dikes

background counting time were 20 s and 10 s, respectively, for each spot. Natural minerals and synthetic oxides were used as standards, including albite for Na, diopside for Si, Ca and Mg, haematite for Fe, orthoclase for K, and synthetic Cr_2O_3, TiO_2, Al_2O_3, MnO and NiO for Cr, Ti, Al, Mn and Ni, respectively. All raw data have been processed an on-line correction using a JEOL-modified ZAF (atomic number, absorption, fluorescence) procedure.

Clinopyroxene trace element determination

Clinopyroxene trace element concentrations were measured by laser ablation on an Agilent 7500a inductively coupled plasma–mass spectrometer (ICP–MS) coupled with a 193 nm Coherent COMPex Pro ArF Excimer laser. Isotopes were measured in a peak-hopping mode, using a

Table 1 Modal compositions of the Dazhuqu mantle peridotites

Sample	Lithology	Major textures	Modal compositions/%			
			Olivine	Orthopyroxene	Clinopyroxene	Spinel
14DZQ08	Harzburgite	protogranular	82.5	14.3	2.3	0.8
14DZQ09	Lherzolite	porphyroclastic	71.4	22.7	5.3	0.6
14DZQ11	Lherzolite	porphyroclastic	73.4	19.1	6.6	1.0
14DZQ12	Lherzolite	protogranular	65.7	26.2	7.3	0.8
14DZQ13	Lherzolite	porphyroclastic	70.0	24.2	5.1	0.7
14DZQ14	Lherzolite	porphyroclastic	70.1	22.8	6.5	0.7
14DZQ15	Lherzolite	porphyroclastic	71.4	22.8	5.1	0.7
14DZQ16	Harzburgite	protogranular	73.2	22.4	3.5	0.9
14DZQ17	Harzburgite	porphyroclastic	71.6	25.0	2.7	0.7
14DZQ18	Harzburgite	porphyroclastic	77.8	18.8	2.7	0.7
14DZQ19	Lherzolite	porphyroclastic	61.0	32.1	6.3	0.6
14DZQ71	Harzburgite	porphyroclastic	80.2	17.4	1.6	0.7
14DZQ72	Harzburgite	porphyroclastic	76.2	17.7	4.9	1.3
14DZQ73	Harzburgite	porphyroclastic	76.3	21.5	1.8	0.4
14DZQ74	Harzburgite	porphyroclastic	70.3	25.6	3.7	0.4
14DZQ75	Harzburgite	porphyroclastic	66.1	31.5	1.9	0.4
14DZQ76	Harzburgite	porphyroclastic	65.3	29.7	4.7	0.3
14DZQ77	Harzburgite	porphyroclastic	80.6	15.1	3.8	0.5
14DZQ78	Harzburgite	porphyroclastic	67.0	31.9	0.7	0.5
14DZQ79	Harzburgite	porphyroclastic	71.7	25.0	2.6	0.6
14DZQ80	Harzburgite	protogranular	84.3	13.5	1.5	0.7
14DZQ81	Harzburgite	porphyroclastic	79.3	18.4	1.7	0.5
14DZQ82	Harzburgite	porphyroclastic	66.6	30.3	2.6	0.5
14DZQ83	Harzburgite	porphyroclastic	73.3	21.8	4.3	0.5
14DZQ84	Harzburgite	porphyroclastic	81.1	12.8	4.8	1.3
14DZQ86	Lherzolite	porphyroclastic	67.5	26.7	5.2	0.6
14DZQ88	Lherzolite	porphyroclastic	76.0	17.3	5.7	1.0
14DZQ90	Lherzolite	porphyroclastic	62.3	31.6	5.4	0.6
14DZQ91	Lherzolite	porphyroclastic	68.2	25.7	5.4	0.8
14DZQ92	Harzburgite	porphyroclastic	69.4	25.7	4.3	0.6
14DZQ93	Harzburgite	porphyroclastic	74.2	22.6	2.3	0.8
14DZQ94	Harzburgite	porphyroclastic	74.2	21.2	3.7	0.9
14DZQ95	Lherzolite	porphyroclastic	69.5	24.6	5.1	0.8

Modal composition estimates are based on systematic petrographic observations and on combined calculations using whole-rock and mineral major element compositions

laser diameter of ca. 120 μm and a repetition rate of 8 Hz. The NIST 610 glass was used as an external standard for calibration and the NIST 612 standard was used for monitoring signal drift. The results of NIST 610 are listed in Online Resource Table S2 and are consistent with the recommended values of Pearce et al. (1997) for all elements analyzed. The relative error for most elements between the measured and recommended values of NIST 610 is very low, with a highest value of 0.74% for U. Calcium (^{43}Ca) was used as an internal standard and the raw data were reduced using the GLITTER 4.0 program (Griffin et al. 2008).

HSE and Re–Os isotope analyses

The HSE contents and Re–Os isotopes were determined by isotope dilution (ID). The detailed procedures have been described by Chu et al. (2009). About 2 g sample powder and appropriate amounts of a ^{187}Re–^{190}Os mixed spike and a ^{191}Ir–^{99}Ru–^{194}Pt–^{105}Pd mixed spike were digested with 3 ml purified concentrated HCl and 6 ml purified concentrated 16 N HNO_3 in a Pyrex® borosilicate glass Carius Tube. After digestion at ~220 °C for about 72 h, Os was extracted from the aqua regia solution into CCl_4 and then back-extracted into HBr followed by purification via microdistillation (Birck et al. 1997). Rhenium, Ir, Ru, Pt and Pd

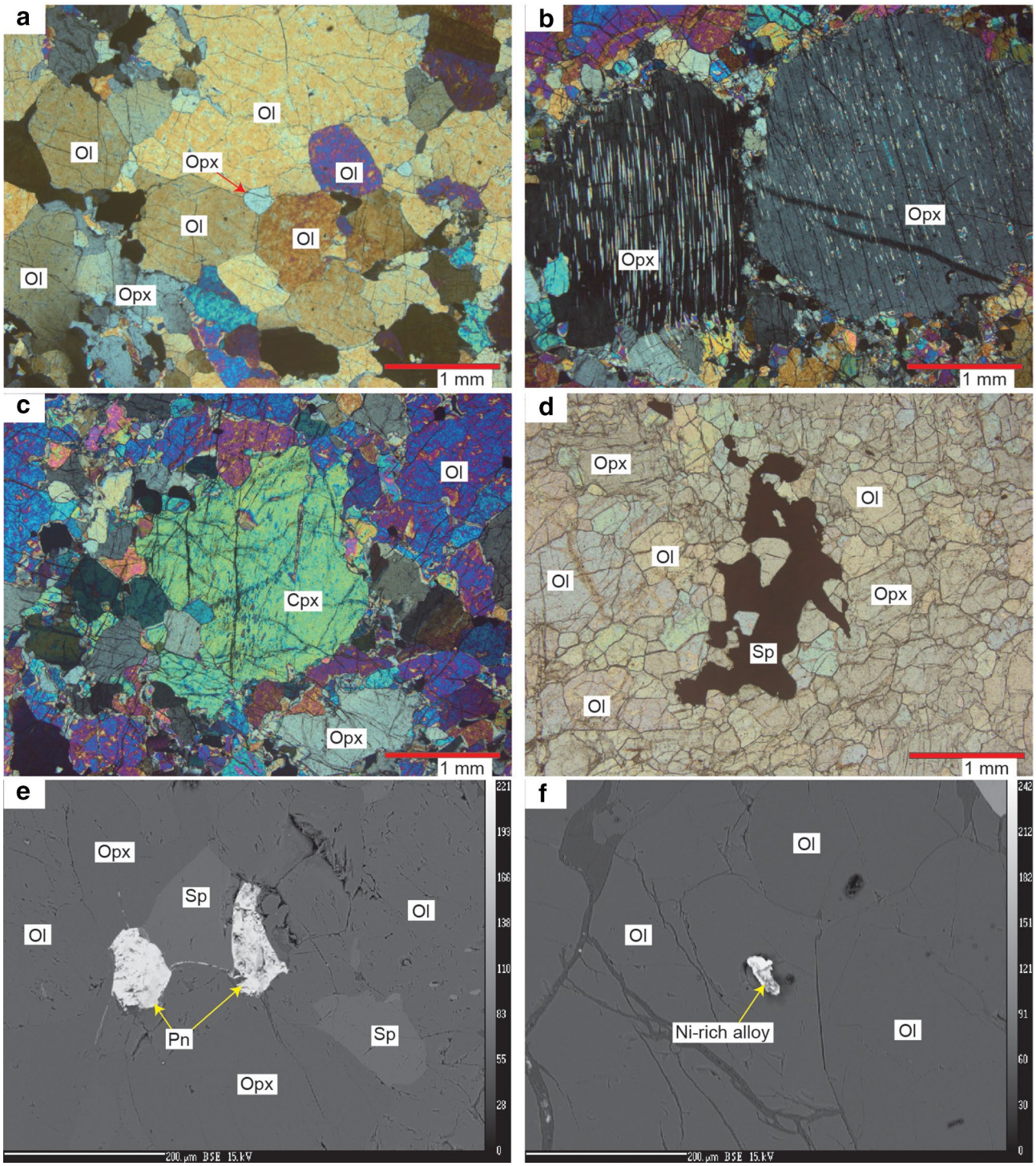

Fig. 3 Photomicrographs and BSE images of the Dazhuqu mantle peridotites. **a** The Dazhuqu harzburgites show a protogranular texture, in which olivine and orthopyroxene display a curvilinear and polygonal shape. Some olivine and orthopyroxene are locally recrystallized and show triple junctions. **b** The Dazhuqu harzubrgites display a porphyroclastic texture, in which orthopyroxene porphyroclasts are surrounded by fine-grained neoblasts. Exsolution lamellae of clinopyroxenes are widely developed in orthopyroxene porphyroclasts. **c** Clinopyroxenes from the Dazhuqu lherzolties display a porphyroclastic texture. **d** Brownish spinels of the Dazhuqu harzburgites commonly have a holly-leaf shape. **e** The Dazhuqu lherzolites typically contain a few amounts of subhedral sulfides (mainly pentlandite). **f** Sulfides are rare in the Dazhuqu harzburgites, which only contain a few grains of Ni-rich alloys included in olivines or orthopyroxenes. Abbreviations are as follows: *Ol* olivine, *Opx* orthopyroxene, *Cpx* clinopyroxene, *Sp* spinel, *Pn* pentlandite

were separated and purified by exchange chromatography using a 2 ml resin (AG 1 × 8, 100–200 mesh) (Walker et al. 2008) for further elution. The Re–Ru, Ir–Pt and Pd fractions were eluted with 6 N HNO_3, 13.5 N HNO_3 and 10 N HCl, respectively. The Re fraction was then purified using a small-size anion exchange column with ~0.1 ml resin. Each fraction of the Re, Ir, Ru, Pt and Pd was heated to dryness and re-dissolved in 1 ml 0.8N HNO_3 for analysis by ICP–MS.

Osmium isotopic compositions were measured at the thermal ionization mass spectrometer (TIMS) Laboratory using a GV Isoprobe-T mass spectrometer. During measurement, Os was loaded onto platinum filaments and $Ba(OH)_2$ was used as an ion emitter. Os isotopic ratios were corrected for oxygen isotope fractionation using the standard oxygen isotope corrections of Nier and online mass fractionation using $^{192}Os/^{188}Os = 3.08271$ and for off-line spike corrections. During analysis, a Johnson-Matthey standard (UMCP) yielded the $^{187}Os/^{188}Os$ ratio of 0.11378 ± 2 (2σ; σ = relative standard deviation; $n = 4$), which is consistent with the result ($^{187}Os/^{188}Os = 0.113791 \pm 15$) analyzed by Shirey and Walker (1998). An international serpentinite standard UB-N was used as an external standard and had a measured Os concentration of 3.90 pg and $^{187}Os/^{188}Os$ ratio of 0.12690 ± 3 (2SE). The in-run precisions for Os isotopic ratios of all samples were better than ±0.2% (2σ). The total procedural blanks were about 0.93–0.97 pg for Os ($n = 2$). Rhenium and other HSE (Ir, Ru, Pt and Pd) were measured at the MC–ICPMS Laboratory using a Thermo Fisher Neptune Plus mass spectrometry. The measured results of UB-N were 3.48 ng for Ir, 7.07 ng for Ru, 7.30 ng for Pt, 5.84 ng for Pd and 0.209 ng for Re, respectively. These values are consistent with the recommended values of UB-N from Meisel and Moser (2004) with Ir = 3.38 ng, Ru = 6.30 ng, Pt = 7.42 ng, Pd = 6.11 ng and Re = 0.206 ng. The total procedural blanks for Ir, Ru, Pt, Pd and Re were 4–10 pg, 18–28 pg, 24–29 pg, 33–37 pg and 2–4 pg, respectively. The in-run precisions for $^{185}Re/^{187}Re$, $^{191}Ir/^{193}Ir$, $^{194}Pt/^{196}Pt$, $^{105}Pd/^{106}Pd$ and $^{99}Ru/^{101}Ru$ were commonly 0.1–0.3% (2RSD). Replicate analyses were conducted on sample 14DZQ12 to check the reproducibility, yielding relative differences of ~1% for $^{187}Os/^{188}Os$ ratio, of ~0.5% for Pd but of ~5–18% for other HSE, which are probably slightly influenced by chemical separation processes.

Results

Whole-rock major element compositions

Whole-rock major element compositions of the Dazhuqu mantle peridotites are listed in Table 2. Most of the studied samples are quite fresh with the LOI less than 1.1 wt.%, but two samples (14DZQ74 and 14DZQ76) have relatively higher LOI values of 1.8–3.2 wt.%. On the whole, these samples have homogeneous Mg# [atomic Mg/ (Mg + Fe)] values of ~0.92 (Table 2). The Dazhuqu harzburgites contain 41.8–45.5 wt.% MgO, 0.4–1.3 wt.% Al_2O_3, 0.5–1.3 wt.% CaO (Fig. 4) and ~0.01 wt.% TiO_2, but negligible Na_2O contents, which are comparable to the most depleted abyssal peridotites [data compilation by Niu (2004)] and the least refractory peridotites from the Izu–Bonin–Mariana (IBM) fore-arc basin (Parkinson and Pearce 1998). Compared to the harzburgites, the Dazhuqu lherzolites have lower MgO (41.8–44.0 wt.%) but higher Al_2O_3 (1.1–1.6 wt.%), CaO (1.4–1.9 wt.%) and TiO_2 (0.01–0.02 wt.%) contents. It is clear that the Dazhuqu lherzolites are less refractory than both the Dazhuqu harzburgites and the IBM fore-arc peridotites (Fig. 4). The Dazhuqu harzburgites and lherzolites both plot parallel to the modeled partial melting trends from Niu (1997). However, most of these samples show lower Al_2O_3 and CaO contents at a given MgO, compared to the compositions assumed by both polybaric near-fractional melting (25–8 kbar) and isobaric batch melting (20 kbar) (Niu 1997; Fig. 4).

Mineral chemistry

Mineral major element average compositions are listed in Online Resource Table S1. Olivines from the Dazhuqu harzburgites have forsterite contents [Fo; 100 × Mg/ (Mg + Fe)] of 90.3–91.3. Coexisting spinels have Cr# [Cr/(Cr + Al)] of ~0.3–0.7 and Mg# of ~0.5–0.7; overall, they contain TiO_2 contents less than 0.1 wt.%. The Dazhuqu lherzolites contain olivines and spinels with compositions overlapping with some of the harzburgites, but the olivine Fo contents (89.7–90.6) and spinel Cr# values (~0.3–0.4) of the lherzolites are both in relatively lower ranges (Fig. 5). In addition, the spinel Cr# of both the Dazhuqu harzburgites and lherzolites display a positive correlation with the olivine Fo contents but a negative correlation with the spinel Mg# (Fig. 5). These spinels share chemical characteristics overlapping with the ranges of both abyssal [see the review by Warren (2016)] and fore-arc peridotites (Parkinson and Pearce 1998; Pearce et al. 2000), with roughly equal numbers of samples plotting out of both fields (Fig. 5). In comparison, spinels from the harzburgites of the Luqu ophiolite (Zhang et al. 2017), which is located about 70 km west to Dazhuqu, have relatively higher Cr# values and plot all within the range of fore-arc peridotites, though most of them are within the range of abyssal peridotites (Fig. 5).

Clinopyroxenes from the Dazhuqu mantle peridotites have relatively low Na_2O contents of 0.04–0.47 wt.% (Fig. 6), which are in the lower end of the abyssal peridotite field (Warren 2016) but are not consistent with the range for continental peridotites (Hellebrand and Snow 2003). It

Table 2 Whole-rock major element compositions (wt.%) of the Dazhuqu mantle peridotites

Sample	Lithology	SiO_2	TiO_2	Al_2O_3	Fe_2O_3t	MnO	MgO	CaO	Na_2O	K_2O	P_2O_5	Cr_2O_3	NiO	LOI	Total	Mg#
14DZQ08	Harzburgite	43.52	0.01	0.56	8.96	0.12	45.48	0.67	0.00	0.01	0.01	0.45	0.33	0.00	100.12	0.92
14DZQ09	Lherzolite	44.30	0.01	1.05	8.86	0.13	43.97	1.40	0.00	0.03	0.00	0.35	0.33	0.00	100.43	0.92
14DZQ11	Lherzolite	43.88	0.02	1.35	8.78	0.13	42.90	1.64	0.00	0.00	0.01	0.39	0.33	0.00	99.42	0.92
14DZQ12	Lherzolite	44.44	0.02	1.38	9.19	0.13	41.77	1.88	0.00	0.00	0.01	0.39	0.30	0.00	99.51	0.91
14DZQ13	Lherzolite	44.03	0.02	1.29	8.90	0.13	43.14	1.38	0.00	0.00	0.01	0.37	0.30	0.00	99.57	0.92
14DZQ14	Lherzolite	44.32	0.02	1.24	8.77	0.13	43.24	1.68	0.00	0.00	0.01	0.41	0.31	0.00	100.13	0.92
14DZQ15	Lherzolite	44.17	0.02	1.20	8.77	0.13	43.35	1.39	0.00	0.00	0.01	0.42	0.30	0.00	99.76	0.92
14DZQ16	Harzburgite	43.98	0.02	1.28	9.21	0.13	44.11	1.06	0.00	0.00	0.01	0.38	0.32	0.00	100.49	0.92
14DZQ17	Harzburgite	44.29	0.01	1.16	8.93	0.13	43.92	0.79	0.00	0.00	0.01	0.46	0.32	0.00	100.02	0.92
14DZQ18	Harzburgite	44.40	0.01	0.60	8.55	0.12	45.10	0.76	0.00	0.00	0.01	0.38	0.32	0.00	100.26	0.92
14DZQ19	Lherzolite	45.27	0.02	1.57	8.74	0.13	42.56	1.79	0.00	0.00	0.01	0.40	0.30	0.00	100.68	0.92
14DZQ71	Harzburgite	44.01	0.01	0.75	8.80	0.12	44.78	0.56	0.00	0.02	0.00	0.38	0.30	0.36	100.09	0.92
14DZQ72	Harzburgite	43.73	0.01	1.19	8.78	0.12	43.49	1.23	0.00	0.01	0.01	0.48	0.29	0.38	99.73	0.92
14DZQ73	Harzburgite	43.41	0.01	0.48	9.06	0.13	45.34	0.57	0.00	0.01	0.01	0.33	0.31	0.00	99.65	0.92
14DZQ74	Harzburgite	43.04	0.01	1.07	9.05	0.13	42.83	1.06	0.00	0.01	0.01	0.32	0.30	1.82	99.65	0.92
14DZQ75	Harzburgite	44.78	0.01	0.72	8.68	0.13	44.09	0.76	0.00	0.01	0.01	0.38	0.30	0.00	99.87	0.92
14DZQ76	Harzburgite	42.79	0.01	0.98	8.61	0.12	41.83	1.25	0.00	0.01	0.00	0.32	0.32	3.24	99.47	0.92
14DZQ77	Harzburgite	42.65	0.01	0.49	8.93	0.13	44.28	0.97	0.00	0.01	0.00	0.33	0.32	1.06	99.18	0.92
14DZQ78	Harzburgite	44.98	0.01	0.40	8.61	0.12	43.75	0.47	0.00	0.01	0.00	0.39	0.30	0.80	99.84	0.92
14DZQ79	Harzburgite	44.23	0.01	0.67	8.93	0.13	44.34	0.73	0.00	0.00	0.00	0.43	0.28	0.00	99.75	0.92
14DZQ80	Harzburgite	43.47	0.01	0.36	8.91	0.12	45.42	0.45	0.00	0.01	0.01	0.41	0.31	0.00	99.48	0.92
14DZQ81	Harzburgite	43.47	0.01	0.48	8.84	0.12	45.45	0.54	0.00	0.01	0.01	0.37	0.31	0.00	99.60	0.92
14DZQ82	Harzburgite	44.07	0.01	0.79	8.99	0.13	43.74	0.79	0.00	0.02	0.01	0.39	0.30	0.00	99.23	0.92
14DZQ83	Harzburgite	43.07	0.01	0.98	8.93	0.12	43.63	1.18	0.00	0.01	0.01	0.35	0.32	0.92	99.53	0.92
14DZQ84	Harzburgite	43.38	0.01	1.01	9.05	0.12	43.76	1.21	0.00	0.01	0.00	0.48	0.29	0.06	99.40	0.92
14DZQ86	Lherzolite	44.79	0.01	1.28	8.58	0.13	42.19	1.45	0.00	0.01	0.01	0.37	0.28	0.34	99.44	0.92
14DZQ88	Lherzolite	44.00	0.01	1.15	8.97	0.13	43.73	1.47	0.00	0.00	0.01	0.38	0.32	0.00	100.18	0.92
14DZQ90	Lherzolite	45.00	0.01	1.41	8.84	0.13	42.87	1.53	0.00	0.01	0.01	0.40	0.31	0.26	100.77	0.92
14DZQ91	Lherzolite	44.69	0.01	1.29	9.00	0.13	43.40	1.49	0.00	0.00	0.01	0.42	0.30	0.02	100.76	0.92
14DZQ92	Harzburgite	44.31	0.01	0.85	8.95	0.13	43.40	1.25	0.00	0.01	0.01	0.40	0.33	0.00	99.65	0.92
14DZQ93	Harzburgite	44.15	0.01	0.71	8.93	0.12	44.61	0.74	0.00	0.00	0.01	0.49	0.14	0.00	99.91	0.92
14DZQ94	Harzburgite	43.54	0.02	1.03	8.93	0.13	43.96	1.17	0.00	0.00	0.01	0.40	0.31	0.00	99.50	0.92
14DZQ95	Lherzolite	44.78	0.01	1.08	8.66	0.12	42.04	1.35	0.00	0.01	0.01	0.45	0.33	0.16	99.01	0.92

LOI loss on ignition; *Mg#* Mg/(Mg + Fe)

should be noted that the correlation of the Na_2O contents in clinopyroxenes and Cr# values in spinels from a few Dazhuqu harzburgites clearly deviates from the modeled fractional melting trend from a Na-rich source (Fig. 6).

Trace element concentrations of clinopyroxenes from the Dazhuqu mantle peridotites measured by *in situ* LA–ICPMS are listed in Online Resource Table S2. Overall, clinopyroxenes from these samples show chondritic to sub-chondritic trace element abundances (Fig. 7a). The REE abundances are much lower than those of depleted mid-ocean ridge basalt mantle (DMM) source and the average composition of abyssal peridotites (Warren 2016). Most of the clinopyroxenes from both the harzburgites and lherzolites display decreasing chondrite-normalized abundances from the heavy REE (HREE) through the middle REE (MREE) and the light REE (LREE), though the latter group in some of the harzburgites shows considerable variation (Fig. 7a). Furthermore, samples with relatively high LREE concentrations also display elevated Sr and Zr contents (Fig. 7b).

HSE and Re–Os isotopic compositions

Whole-rock HSE and Re–Os isotopic compositions of 21 samples of the Dazhuqu mantle peridotites are shown in Table 3. All Dazhuqu samples have consistent and relatively flat IPGE (Ir-group platinum group elements; i.e., Os, Ir and Ru) patterns (Fig. 8) when normalized to CI chondrite (Horan et al. 2003). Their measured Os/Ir and Ru/Ir

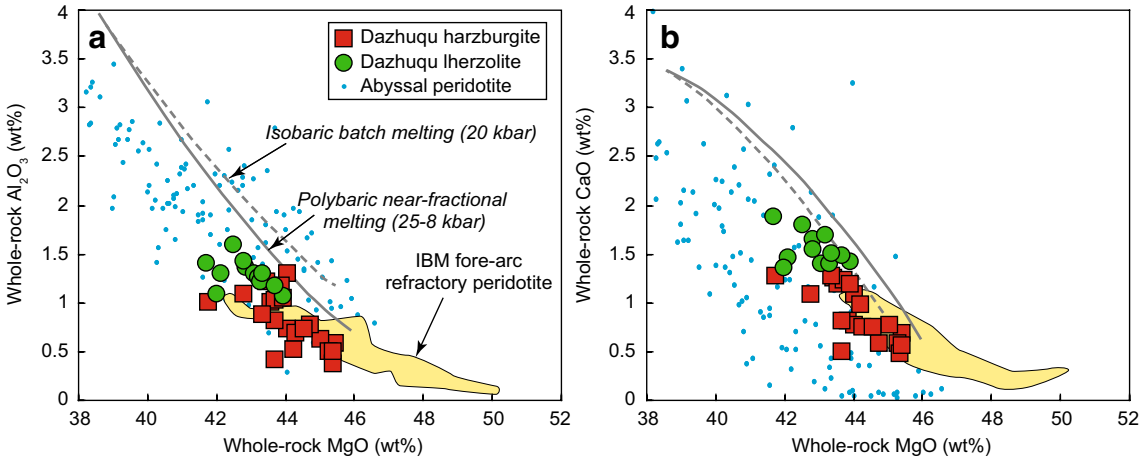

Fig. 4 Plots of whole-rock MgO against Al_2O_3 and CaO contents of the Dazhuqu mantle peridotites. The data plotted are recalculated to an anhydrous composition. Fields of the Izu–Bonin–Mariana (IBM) fore-arc refractory peridotites are after Parkinson and Pearce (1998). Data of abyssal peridotites are from the compilation by Niu (2004). The polybaric near-fractional (1% melt porosity) melting (with initial pressures from 25 kbar) and isobaric batch melting (at pressure = 20 kbar) curves are after Niu (1997)

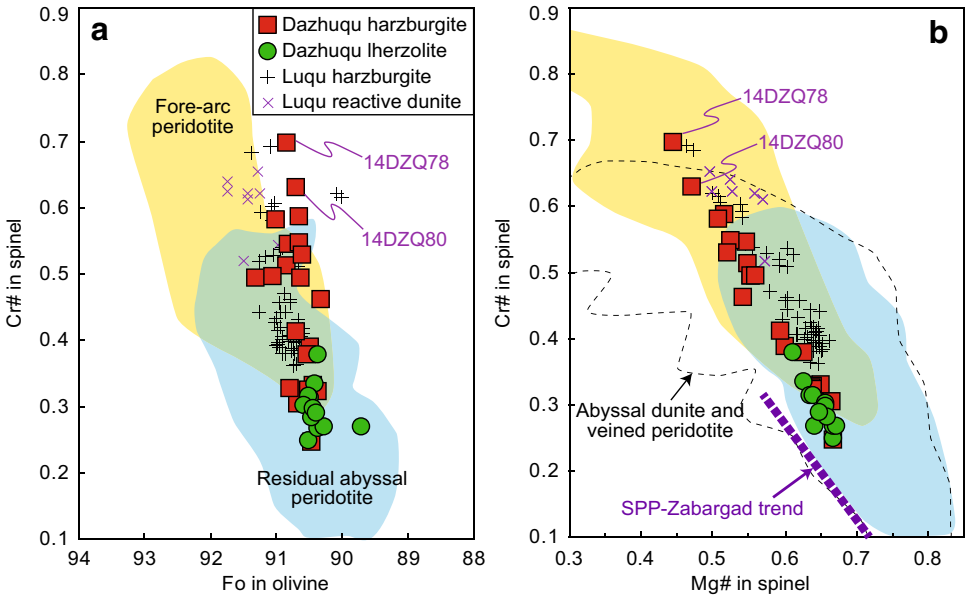

Fig. 5 Spinel Cr# versus olivine Fo (**a**) and spinel Mg# (**b**) of the Dazhuqu mantle peridotites. Fields of residual abyssal peridotite, abyssal dunite and veined peridotite are after the review in Warren (2016) and fields of fore-arc peridotite are from Parkinson and Pearce (1998) and Pearce et al. (2000). Data of the Luqu harzburgite and reactive dunite are from Zhang et al. (2017). The samples of 14DZQ78 and 14DZQ80 are the only two Dazhuqu samples in this study with spinel Cr# above 0.6

ratios (non-normalized) range from 0.7 to 1.6 and 0.9–1.6, respectively. Most Dazhuqu peridotites also have relatively flat patterns in PPGE (Pd-group PGE; i.e., Pt and Pd) and Re, but seven harzburgite samples show variable PPGE patterns and also moderate to strong depletion in Re (Fig. 8). In addition, two out of seven harzburgites have elevated Pt and particularly Pd abundances relative to the recommended values of primitive upper mantle (PUM; Meisel et al. 2001). As a whole, the measured Pt/Ir, Pd/Ir and Re/Ir ratios (non-normalized) of the Dazhuqu mantle peridotites range from 0.5 to 2.4, 0.5–3.6 and 0.04–1.0, respectively.

The Dazhuqu mantle peridotites contain 2.55–5.64 ppb Os and 0.01–0.37 ppb Re (Table 3), yielding $^{187}Re/^{188}Os$ ratios of 0.01–0.35. They have $^{187}Os/^{188}Os$ ratios of 0.11836–0.12922 (Fig. 9a) that are similar to the values reported for mantle peridotites from the Purang and Dongbo ophiolites in the western segment of the YZSZ (Gong et al. 2016; Liu et al. 2012; Niu et al. 2015), but are lower than the recommended value (0.1296 ± 0.0008) of PUM (Meisel et al. 2001). In addition, a roughly positive covariation exists between $^{187}Re/^{188}Os$ and $^{187}Os/^{188}Os$ ratios for most Dazhuqu peridotites, but some harzburgite samples deviate, either above or below, from the correlation (Fig. 9a). The $^{187}Os/^{188}Os$ ratios do not show a correlation with whole-rock Al_2O_3 contents (Fig. 9b). Re

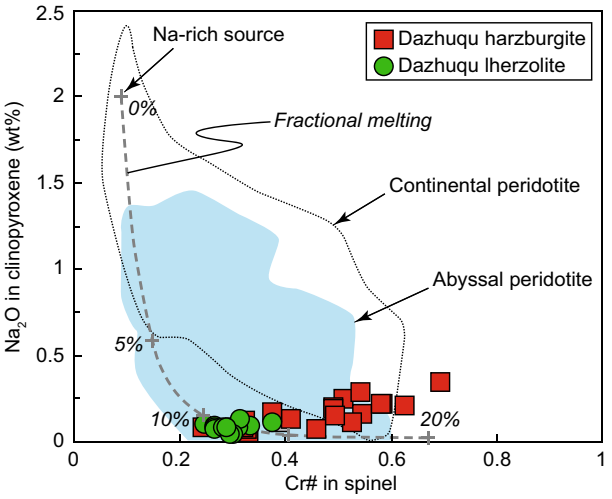

Fig. 6 Clinopyroxene Na_2O versus spinel Cr# of the Dazhuqu mantle peridotites. The fractional melting trend (with 1% melting increments) and the field of continental peridotite are according to the review in Hellebrand and Snow (2003); the field of abyssal peridotite is after the data compilation in Warren (2016)

depletion ages (T_{RD}) of the Dazhuqu peridotites calculated relative to PUM range from 0.06 to 1.66 Ga (Table 3).

Discussion

Garnet-facies initial melting and melt–rock interaction

The Dazhuqu mantle peridotites show variably refractory compositions that plot parallel to the modelled partial melting curves (Fig. 4), indicating that they must have experienced variable degrees of melting. However, the Dazhuqu samples in this study mostly contain lower Al_2O_3 and CaO at a given MgO and could not be perfectly modeled neither by polybaric fractional melting nor by isobaric batch melting (Niu 1997). Petrographic observations showed that orthopyroxene porphyroclasts from the Dazhuqu peridotites display extremely irregular outlines and are commonly surrounded by fine-grained olivine neoblasts (Fig. 3b), indicating orthopyroxene resorption and replacement by olivine. This feature has been widely interpreted as resulting from porous flow migration and interaction of peridotites with pyroxene-undersaturated melts (Rampone et al. 2008; Seyler et al. 2007). Therefore, the deviation from the partial melting trends could be ascribed to melt–rock interaction, resulting in the addition of olivine (Niu 1997).

Using the empirical equation [$F = 10 \times \ln(\mathrm{Cr\#_{spinel}}) + 24$, F here means the extent of melting in percent] established by Hellebrand et al. (2001), it can be estimated that the Dazhuqu peridotites have been subjected to 10–18% of fractional melting of a depleted mantle source. Similarly, in the diagram of spinel Cr# versus clinopyroxene Yb (Fig. 10a), the majority of the Dazhuqu samples plot close to the pure fractional melting trend (Liu et al. 2008) and yield 10–20% of partial melting. However, these samples are characterized by steeper MREE to HREE patterns (Fig. 7a) relative to the average composition of abyssal peridotites (Warren 2016) and the modelled fractional melting trend (Hellebrand et al. 2002). This observation is of particular importance for evaluating the potential role of residual garnet during initial melting, which has been proposed in both abyssal and ophiolitic peridotites (Brunelli et al. 2006; Gong et al. 2016; Hellebrand et al. 2002;

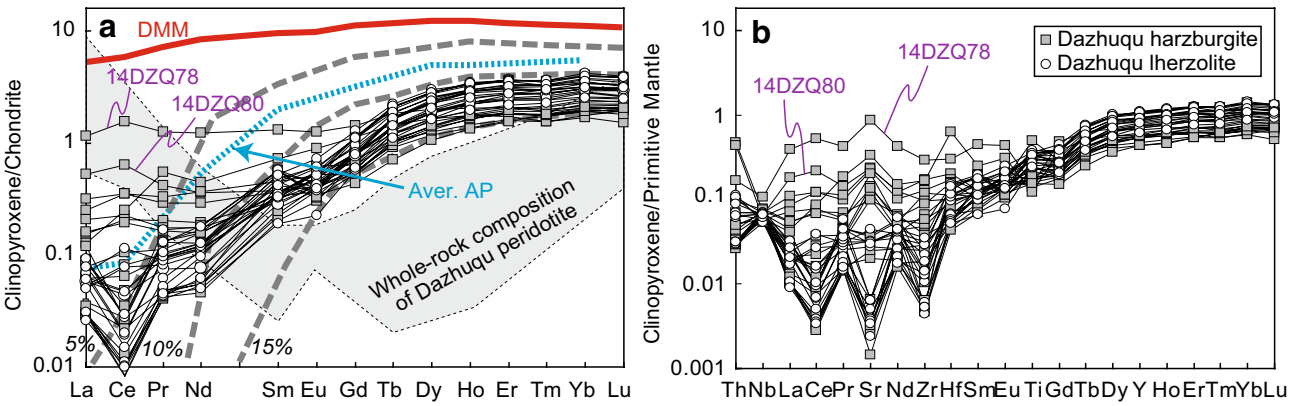

Fig. 7 Chondrite-normalized REE (**a**) and primitive mantle-normalized trace element (**b**) patterns of clinopyroxenes from the Dazhuqu mantle peridotites. The data are measured by in situ LA–ICPMS. REE of clinopyroxene after 5%, 10% and 15% fractional melting from a depleted MORB mantle (DMM) source (Workman and Hart 2005) is shown, using the modeled results described in Hellebrand et al. (2002). The field of whole-rock compositions of the Dazhuqu mantle peridotites is after Xia et al. (2003). The average composition of abyssal peridotites (Aver. AP) from Warren (2016) is shown for comparison. Chondrite and primitive mantle values are proposed by Sun and McDonough (1989)

Table 3 Re–Os isotopes and HSE compositions of the Dazhuqu mantle peridotites

Sample	Lithology	Os (ppb)	Ir (ppb)	Ru (ppb)	Pt (ppb)	Pd (ppb)	Re (ppb)	$^{187}Re/^{188}Os$	$^{187}Os/^{188}Os$	2SE	Blk%	T_{RD} (Ma)
14DZQ08	Harzburgite	n.d	4.51	8.86	9.00	7.33	0.259	n.d	n.d	n.d	n.d	n.d
14DZQ12	Lherzolite	5.51	4.37	9.12	11.13	8.75	0.296	0.259	0.12634	0.00019	0.008	485
14DZQ12R	Lherzolite	4.78	3.60	8.19	10.38	8.79	0.282	0.284	0.12752	0.00010	0.010	309
14DZQ13	Lherzolite	n.d	4.07	8.08	7.89	5.81	0.232	n.d	n.d	n.d	n.d	n.d
14DZQ14	Lherzolite	5.04	4.17	8.71	8.64	7.11	0.361	0.345	0.12830	0.00007	0.009	193
14DZQ15	Lherzolite	5.00	4.28	8.36	8.54	6.81	0.284	0.274	0.12588	0.00003	0.009	553
14DZQ18	Harzburgite	5.47	4.59	8.60	9.32	8.93	0.070	0.061	0.12679	0.00003	0.008	418
14DZQ19	Lherzolite	5.63	4.89	9.57	9.20	8.01	0.373	0.319	0.12711	0.00002	0.008	371
14DZQ71	Harzburgite	2.55	3.69	4.86	7.47	3.98	0.082	0.154	0.11836	0.00004	0.018	1655
14DZQ73	Harzburgite	4.54	3.67	7.25	8.45	6.87	0.218	0.231	0.12727	0.00005	0.010	346
14DZQ75	Harzburgite	4.39	3.73	7.47	16.91	16.69	0.296	0.326	0.12922	0.00002	0.011	57
14DZQ77	Harzburgite	4.40	3.81	7.46	7.38	6.96	0.236	0.258	0.12621	0.00006	0.011	504
14DZQ78	Harzburgite	n.d	3.91	5.58	15.13	11.31	0.018	n.d	n.d	n.d	n.d	n.d
14DZQ79	Harzburgite	4.65	4.09	8.17	7.90	6.78	0.249	0.258	0.12732	0.00003	0.010	340
14DZQ80	Harzburgite	3.37	3.28	4.85	10.75	2.95	0.010	0.015	0.12501	0.00003	0.014	681
14DZQ81	Harzburgite	5.64	3.52	7.62	5.28	2.14	0.011	0.009	0.12414	0.00001	0.008	810
14DZQ82	Harzburgite	3.51	3.39	n.d	8.27	6.17	n.d	n.d	0.12708	0.00003	0.013	375
14DZQ88	Lherzolite	3.66	3.31	6.52	7.25	6.81	0.257	0.338	0.12829	0.00002	0.013	195
14DZQ91	Lherzolite	4.55	4.00	7.68	8.45	7.55	0.333	0.353	0.12720	0.00002	0.010	358
14DZQ92	Harzburgite	n.d	4.03	8.11	8.00	7.50	0.249	n.d	n.d	n.d	n.d	n.d
14DZQ93	Harzburgite	4.88	4.23	8.17	8.94	6.63	0.203	0.200	0.12546	0.00002	0.010	615
14DZQ94	Harzburgite	4.74	4.17	8.48	7.52	5.75	0.180	0.183	0.12448	0.00004	0.010	760
BLK	Blank	0.00097	0.004	0.018	0.0285	0.037	0.002					
BLK	Blank	0.00093	0.010	0.028	0.0238	0.033	0.004					
UB-N	Serpentinite standard	3.90	3.48	7.07	7.30	5.84	0.209	0.259	0.12690	0.00003	0.012	402

R replicate analysis, T_{RD} is calculated relative to primitive upper mantle (PUM) (Meisel et al. 2001), *Blk%* Os (Blank)/Os (sample) × 100, where Os (Blank) is an average result of the measured blank samples [(0.00097 + 0.00093)/2], *n.d.* not determined

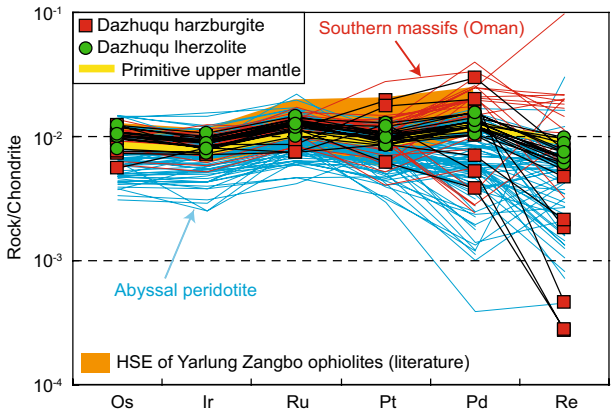

Fig. 8 CI chondrite-normalized highly siderophile element (HSE) patterns of the Dazhuqu mantle peridotites. Data of primitive upper mantle (PUM) and chondrite are from Meisel et al. (2001) and Horan et al. (2003), respectively. Data of the mantle peridotites from Oman southern massifs are from Hanghøj et al. (2010) and Lorand et al. (2009), and data of abyssal peridotites are after the compilation by Day et al. (2017) with three highly fractionated samples excluded. The field of HSE data of the Yarlung Zangbo ophiolites in the literature is after Dai et al. (2011) and references therein

Hellebrand and Snow 2003; Zhang et al. 2017). When garnet breaks down as peridotites rise into the spinel stability field, the HREE that had been hosted in the garnet will be redistributed between the minerals of a spinel peridotite, yielding an equilibrium clinopyroxene with higher HREE concentrations and lower Sm/Yb ratio (Hellebrand et al. 2002). In the $(Sm/Yb)_N$ versus Yb_N diagram [Fig. 11; N: chondrite-normalization by Anders and Grevesse (1989)], comparison with the peridotite melting model of Hellebrand et al. (2002) suggests that the majority of Dazhuqu peridotites have experienced 0–6% garnet-facies melting followed by 10–18% spinel-facies melting. Garnet + spinel facies melting has also been identified in mantle peridotites from the Luqu ophiolite (Fig. 11), which, in comparison, have been subjected to relatively higher degrees of melting than the Dazhuqu peridotites (Zhang et al. 2017). It should be noted that some Dazhuqu samples plot above the modelled melting trend of Hellebrand et al. (2002) (Fig. 11), indicating modification by late-stage refertilization processes, i.e., melt–rock interaction (Brunelli et al. 2006; Hellebrand et al. 2002).

Melt–rock interaction experienced by mantle peridotites can be modeled both qualitatively and quantitatively. Clinopyroxenes in several Dazhuqu peridotites, particularly harzburgites, show enrichment in some incompatible elements (such as LREE, Sr, Zr, Hf and Ti), though most of them display LREE-depleted patterns (Fig. 7). In the diagram of $(Ce/Yb)_N$ versus Yb_N of clinopyroxene, the Dazhuqu peridotites do not follow the fractional melting trend for both spinel- and garnet-facies (Brunelli et al. 2006), but deviate to high Ce/Yb ratios (Fig. 10b). This indicates that the Dazhuqu samples have experienced late-stage enrichment after melt depletion, which resulted in the elevated Ce contents of clinopyroxenes. Clinopyroxene $(Ce/Yb)_N/Yb_N$ is consistent with variably depleted residual clinopyroxene refertilized by a quasi-instantaneous melt extracted after ~ 12% source partial melting (Fig. 10b; Brunelli et al. 2006).

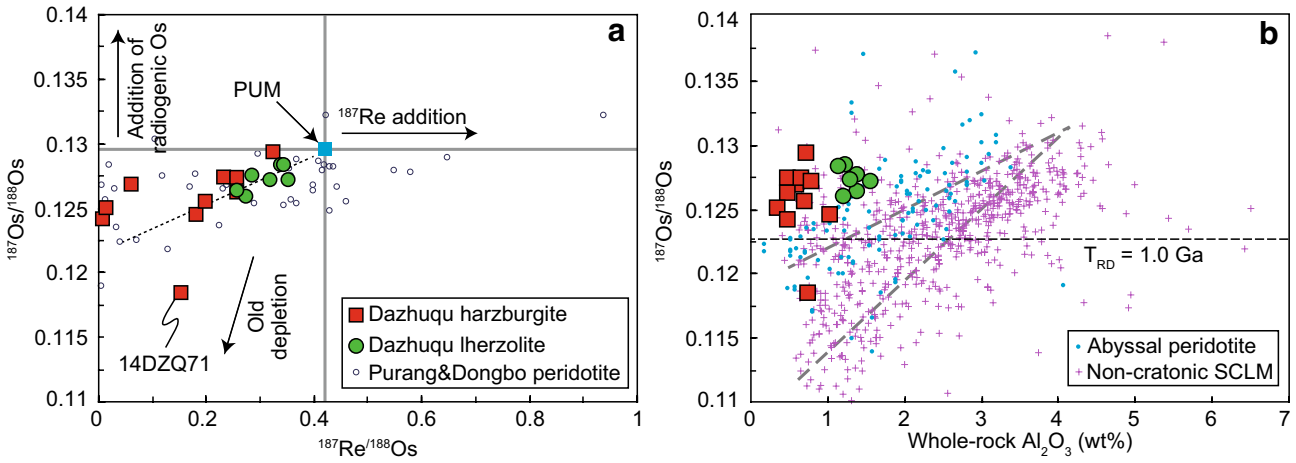

Fig. 9 Re-Os isotopes of the Dazhuqu mantle peridotites. Data of primitive upper mantle (PUM) are from Meisel et al. (2001). Data of the Purang and Dongbo ophiolitic peridotites are from Gong et al. (2016), Liu et al. (2012) and Niu et al. (2015). Data of abyssal peridotites and of non-cratonic SCLM xenoliths are after the compilations by Day et al. (2017) and Luguet and Reisberg (2016), respectively. Dashed lines in Fig. 9b represent two rough positive correlations between $^{187}Os/^{188}Os$ ratio and whole-rock Al_2O_3 content of the non-cratonic SCLM xenoliths

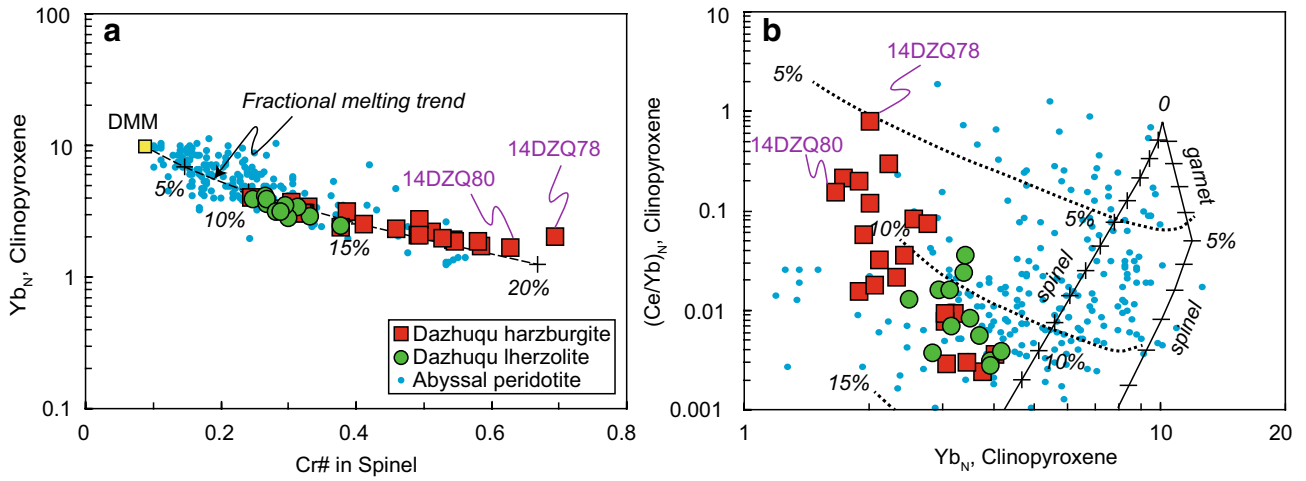

Fig. 10 **a** Clinopyroxene Yb_N versus spinel Cr# of the Dazhuqu mantle peridotites. The fractional melting trend is from Liu et al. (2008). **b** Clinopyroxene $(Ce/Yb)_N$ versus Yb_N of the Dazhuqu mantle peridotites. The fractional melting trends (solid lines) for both spinel and garnet facies are after Brunelli et al. (2006) and Hellebrand et al. (2002). A quantitative calculation for refertilization has been carried out, comparing the refertilization model described by Brunelli et al. (2006). The modelled compositional paths (dashed lines) are followed by a variably depleted residual clinopyroxene refertilized with quasi-instantaneous melts extracted after 5, 10 and 15% source partial melting. Detailed parameters for melting and refertilization modeling are listed in Online Resource Appendix I. Data of abyssal peridotites are after the review in Warren (2016)

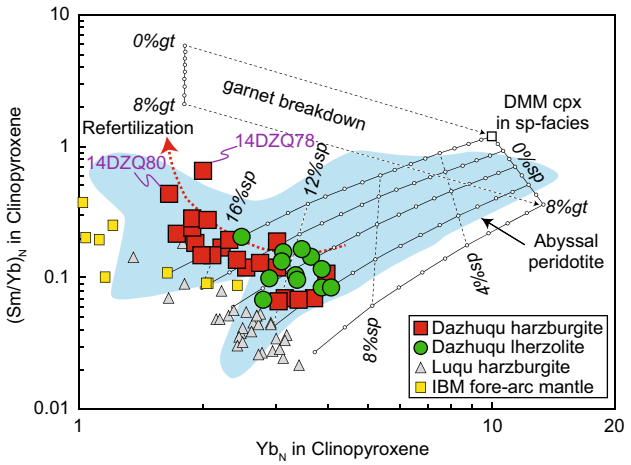

Fig. 11 Clinopyroxene $(Sm/Yb)_N$ versus $(Yb)_N$ of the Dazhuqu mantle peridotites. The trajectories of melting and fields of abyssal peridotites are from Hellebrand et al. (2002). The modeled melting curves describe a three-step process: (1) melting in the garnet stability field, (2) garnet breakdown, (3) melting in the spinel stability field. The labels on the melting curves represent percent melting in the garnet or spinel stability fields. Parameters for melting modeling are after Hellebrand et al. (2002) (Appendix I). Data of the Luqu peridotites are from Zhang et al. (2017), and IBM fore-arc mantle from Parkinson and Pearce (1998) and Chen and Zeng (2007). The refertilization trend (the red dashed arrow) refers to the modeling result from Brunelli et al. (2006) and Hellebrand et al. (2002). Data of chondrite are from Anders and Grevesse (1989). *Sp* spinel, *gt* garnet, *cpx* clinopyroxene

The effects of melting and melt–rock interaction on HSE abundances

It is well known that HSE concentrations of the residual mantle are predominantly controlled by sulfide stability because of the extremely high metal/silicate partition coefficient (e.g., Brenan et al. 2016; Luguet and Reisberg 2016). Due to the stability of sulfides (or alloys or oxides) at low degrees of partial melting, the concentrations of HSE in the residual mantle would increase but their patterns do not change significantly. At larger degrees (> 15–20%) of partial melting, PPGE and Re behave incompatibly whereas IPGE still behave compatibly (Büchl et al. 2002; Keays 1995; Lorand et al. 1999; Morgan 1986), resulting in fractionated HSE patterns. These hypotheses are consistent with the sulfide petrography and HSE patterns of the Dazhuqu mantle peridotites. The Dazhuqu lherzolites typically contain a few (< 1%) subhedral sulfides (mainly pentlandite; Fig. 3e), which is consistent with the sulfide stability at a low extent of melting (i.e., ~ 10–14%). In contrast, sulfides have been rarely discovered in the Dazhuqu harzburgites, which only contain a few grains of Ni-rich alloys (Fig. 3f). This indicates the almost complete consumption of sulfides from the harzburgites at high degrees of melting up to 20%. The sulfide petrography is in a good agreement with the flat HSE patterns of the Dazhuqu lherzolites and the PPGE- and Re-depleted patterns of a few harzburgites (Fig. 8). All but three Dazhuqu samples have consistent Ru/Ir ratios (Fig. 12a); they can be explained by batch melting from PUM, as modeled by van Acken et al. (2010), assuming monosulfide solid

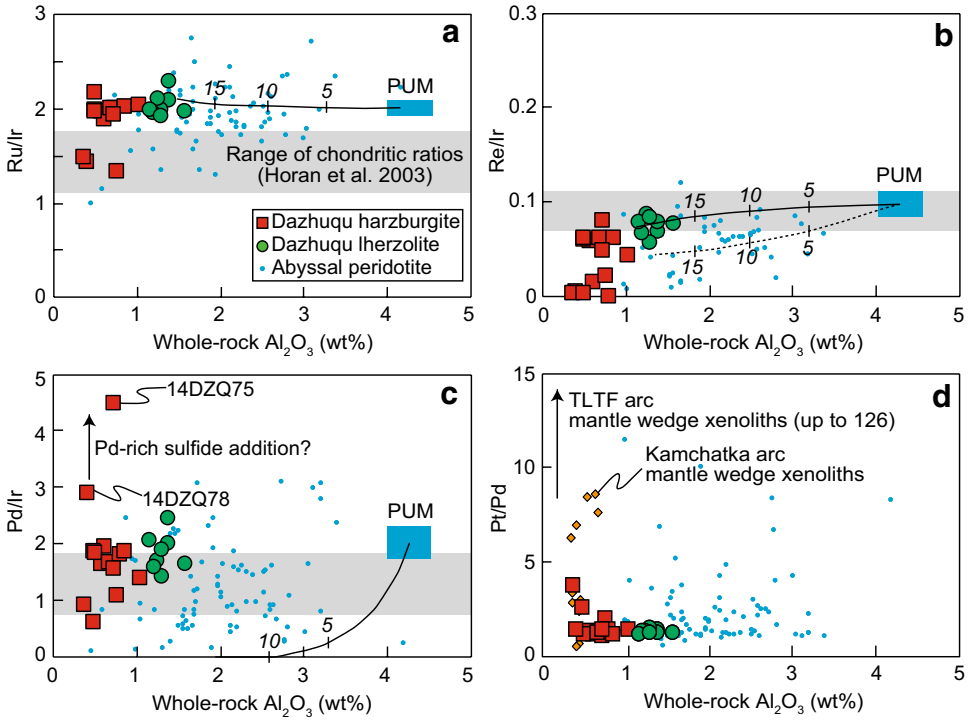

Fig. 12 Measured **a** Ru/Ir, **b** Re/Ir, **c** Pd/Ir and **d** Pt/Pd (non-normalized) versus whole-rock Al_2O_3 correlation diagrams of the Dazhuqu mantle peridotites. Partial melting modeling from van Acken et al. (2010) are shown in **a**–**c** for comparison, where solid lines represent residual peridotite compositions after partial batch melting assuming monosulfide solid solution (mss)–sulfide melt equilibrium (fractional melting trend is similar and not shown), and dashed line in **b** assuming moderately incompatible bulk partitioning of Re. The PUM composition used by the modeling of van Acken et al. (2010) was after Becker et al. (2006). Ranges of chondritic Ru/Ir, Re/Ir and Pd/Ir ratios are after Horan et al. (2003), while the abyssal peridotite compositions are after the compilation by Day et al. (2017). Data of mantle wedge xenoliths from the Kamchatka arc and the trend of those from the Tabar–Lihir–Tanga–Feni (TLTF) arc are after Kepezhinskas and Defant (2001) and McInnes et al. (1999), respectively

solution (mss)–sulfide melt equilibrium. In contrast, the Re/Ir ratios of the Dazhuqu samples decrease sharply at a high extent (> ~ 20%) of melting (Fig. 12b) and deviate from the model of van Acken et al. (2010). This suggests the efficient removal of relatively incompatible Re during melt depletion. As for the Pd/Ir ratio versus whole-rock Al_2O_3 diagram (Fig. 12c), all Dazhuqu samples deviate clearly from the mss–sulfide liquid melting model, a feature that is probably ascribed to the non-consideration of phases (such as alloys and oxides) other than sulfides (van Acken et al. 2010). It should be noted that two Dazhuqu harzburgites (14DZQ75 and 14DZQ78) have elevated Pd/Ir ratio with respect to the other samples (Fig. 12c). The Pd enrichment may be a common feature of the Yarlung Zangbo ophiolitic mantle [Fig. 8; data from this study and Dai et al. (2011) and references therein]. This feature has been also reported for the Oman and Ligurian ophiolitic peridotites and for some abyssal (MARK area) and continental peridotites (Hanghøj et al. 2010; Lorand et al. 2009; Luguet et al. 2003, 2004; Pearson et al. 2004). A possible mechanism is the refertilization of the Pd-depleted residual mantle by Pd-rich, S-saturated Cu–Ni sulfide melts (Lorand et al. 2009; Luguet and Reisberg 2016). This implies a ubiquitous melt–rock interaction between the Yarlung Zangbo upper mantle and Pd-rich sulfide melts, though the interactions are typically in a small volume (Luguet and Reisberg 2016).

Ancient Os isotope signals: SCLM or mantle heterogeneity?

Re–Os isotope systematics provide critical information for constraining the nature and time of melt depletion processes in mantle peridotites, particularly for their ancient depletion signals, and are robust against late-stage metasomatism and contamination processes with respect to lithophile isotope systems (e.g., Sm–Nd and Rb–Sr) (Rudnick and Walker 2009). All studied Dazhuqu mantle peridotites have unradiogenic $^{187}Os/^{188}Os$ ratios (0.11836–0.12922) relative to PUM (Meisel et al. 2001), yielding Re depletion ages, i.e., minimum ages of melt extraction, of 0.06–1.66 Ga (Table 3). All but one Dazhuqu samples plot within the range previously reported for mantle peridotites from other ophiolitic massifs along the YZSZ (Fig. 9a), which are also within the field defined by abyssal peridotites (Fig. 9b). Sample

14DZQ71 has the lowest $^{187}Os/^{188}Os$ ratio (i.e., 0.11836) among all reported whole-rock data for mantle peridotites from the YZSZ, which yields a very old T_{RD} age of 1.66 Ga. This sample stands out from the other samples, which all have $^{187}Os/^{188}Os$ ratios clustered between 0.1241 and 0.1292 and have T_{RD} ages younger than 810 Ma (Table 3; Fig. 9a). The highly depleted Os isotopic composition of the sample 14DZQ71 is somewhat like ancient Os isotope signals preserved in a few abyssal peridotites (Alard et al. 2005; Brandon et al. 2000; Day et al. 2017; Harvey et al. 2006; Lassiter et al. 2014; Liu et al. 2008; Snow and Reisberg 1995) and in ophiolites (Alard et al. 2005; Büchl et al. 2002; Gong et al. 2016; Liu et al. 2012; Snow et al. 2000; van Acken et al. 2008). For example, highly depleted $^{187}Os/^{188}Os$ ratios with T_{RD} ages up to 2.66 Ga have been observed in the sulfides from the Ligurian ophiolitic peridotites (Alard et al. 2005). Old depleted components recorded by abyssal and ophiolitic peridotites are typically explained by two processes (see Rampone and Hofmann (2012) for a review). One hypothesis attributes ancient signatures to preservation of refractory domains in the heterogeneous asthenospheric mantle that have avoided erasure by mantle convection (i.e., mantle heterogeneity; Liu et al. 2008). Another hypothesis suggests that depleted domains result from SCLM slices "stranded" in the asthenosphere during continental rifting and break-up (e.g., Boillot et al. 1989; Müntener and Manatschal 2006; O'Reilly et al. 2009). The second model is best manifested by the St Peter-Paul and Sal Island peridotites (Atlantic Ocean) (Bonatti 1990; Coltorti et al. 2010), the peridotite bodies from the Zabargad Island (Red Sea) (Snow and Schmidt 1999) and the Alpine–Apennine ophiolitic peridotites (Snow et al. 2000; van Acken et al. 2008). For example, the St Peter-Paul peridotites systematically contain lower spinel Cr# and Mg# values and orthopyroxene Al_2O_3 and clinopyroxene Na_2O contents relative to the abyssal peridotites from the Mid-Atlantic Ridge, but comparable to those of the Zabargad peridotite bodies. Therefore, the St Peter-Paul peridotites are thought to be relics of sub-continental mantle left behind during the opening of the equatorial Atlantic (Bonatti 1990), as is the case for the northern and central part of the Zabargad peridotite bodies, which were interpreted as ancient continental lithospheric mantle left by the Red Sea Rift (Snow and Schmidt 1999). Similarly, some old domains within the Alpine–Apennine ophiolites are widely considered as orogenic peridotites trapped in the Jurassic Tethys Ocean (Müntener et al. 2010; Rampone et al. 1995).

The following lines of evidence, however, argue against that this old Dazhuqu mantle peridotite represents an isolated slice of SCLM. First, sub-continental mantle is characterized by the existence of aluminium- and iron-rich spinels, as is the case for the St Peter-Paul (Bonatti 1990) and Zabargad (Bonatti et al. 1986) peridotites. As shown is Fig. 5b, the St Peter-Paul and Zabargad mantle peridotites contain both relatively lower spinel Cr# and Mg# [SPP-Zabargad trend; according to the data compilation by Bonatti (1990)] than residual abyssal peridotites. In this respect, the Al–Fe enrichment of the SPP-Zabargad trend is quite different from the mineral chemical features of the Dazhuqu peridotites, which display chromium and magnesium enrichments in spinels that are comparable to residual abyssal peridotites (Fig. 5b). On the other hand, the majority of abyssal peridotites contain a relatively lower sodium content with respect to continental peridotites at a given spinel Cr# (Hellebrand and Snow 2003), though there is a large overlap between the two, as is shown in Fig. 6 of this study. Continental peridotites and some abyssal peridotites clearly deviate from the fractional melting curve modeled from a Na-rich source by Hellebrand and Snow (2003) (Fig. 6), which could be interpreted as sodium metasomatism even at high pressure in the spinel stability field (Müntener et al. 2010). The Dazhuqu peridotites from this study have extremely low clinopyroxene Na_2O and plot along the fractional melting curve, though a few harzburgites contain relatively higher clinopyroxene Na_2O due to melt refertilization (Fig. 6). It indicates that the Dazhuqu samples are residuals of low-pressure melt extraction and are comparable to most abyssal peridotites (Hellebrand and Snow 2003; Müntener et al. 2010).

Second, we here point out an Os-related indicator for distinguishing the Dazhuqu peridotites from typical non-cratonic SCLM. Numerous studies have focused on potential correlations between chemical fertility indexes (e.g., whole-rock Al_2O_3 content, clinopyroxene Yb abundance and spinel Cr# value) and isotopic (Os and Hf) ratios (Bizimis et al. 2007; Day et al. 2017; Rampone and Hofmann 2012; Reisberg and Lorand 1995; Stracke et al. 2011; Warren et al. 2009). In a prior study, Reisberg and Lorand (1995) present two examples of striking correlations between $^{187}Os/^{188}Os$ ratio and whole-rock Al_2O_3 content in orogenic peridotites (i.e., the Ronda and Eastern Pyrenean ultramafic massifs). These correlations are most simply explained as isochron analogues with Al_2O_3 proportional to Re/Os (Reisberg and Lorand 1995). Data compilation of non-cratonic SCLM xenoliths from Luguet and Reisberg (2016) has indeed yielded two rough positive correlations between $^{187}Os/^{188}Os$ ratio and whole-rock Al_2O_3 content (Fig. 9b). For non-cratonic SCLM xenoliths, the slope of correlations between $^{187}Os/^{188}Os$ and whole-rock Al_2O_3 probably depends on age, that is, young SCLM would be expected to show an approximately flat trend (Luguet and Reisberg 2016). Interestingly, such correlations have also been observed in present-day abyssal peridotites (Day et al. 2017; Warren et al. 2009). In these cases, the presence of old, refractory mantle domains in the MORB source was interpreted as evidence for a SCLM affinity (Rampone and Hofmann 2012; Stracke et al. 2011). Systematic examination of the

Dazhuqu mantle peridotites in this study, however, indicates that no clear correlations between $^{187}Os/^{188}Os$ and whole-rock Al_2O_3 (Fig. 9b) and clinopyroxene Yb (not shown here) exist in these samples. In addition, it is evident that the sample (14DZQ71) with the lowest $^{187}Os/^{188}Os$ ratio does not correspond to the sample with the lowest whole-rock Al_2O_3 and clinopyroxene Yb contents. It is clear that non-cratonic SCLM xenoliths with Os characteristics similar to the Dazhuqu samples can indeed be found, but such SCLM samples are rare. In contrast, the Dazhuqu samples studied all plot within the range of abyssal peridotites (data compilation from Day et al. (2017)) (Fig. 9b). These results argue that an abyssal peridotite affinity for the Dazhuqu samples is much more likely, though their Os isotopic compositions could in theory be consistent with both continental and oceanic affinities. Hence, we conclude, based on all lines of evidence, that the Dazhuqu peridotites are less likely to be samples of isolated sub-continental slices stranded in the oceanic asthenosphere. They represent, in the strict sense, residues of heterogeneous oceanic mantle with preservation of small amounts of old depleted domains, which have experienced ancient melting. These old mantle domains escaped homogenization by asthenospheric convective mixing, as was previously suggested to explain the case of ancient and highly heterogeneous abyssal peridotites beneath the Gakkel Ridge (Liu et al. 2008).

Neo-Tethyan sub-oceanic mantle

Some studies have identified the Xigaze ophiolitic peridotites (including the Dazhuqu massif) as fore-arc peridotites (Dai et al. 2013; Dubois-Côté et al. 2005; Dupuis et al. 2005a; Xia et al. 2003; Xiong et al. 2017). This hypothesis was based mainly on (1) the refractory nature and high degree of melting and (2) the U-shaped whole-rock REE patterns of these mantle peridotites. The Dazhuqu peridotite samples comprise ~ 1/3 lherzolite, though harzburgite is the major rock type (Table 1). One interpretation of this could be that the extent of melting of the Dazhuqu peridotites may be less than typical fore-arc peridotites, which consist mainly of harzburgite (Parkinson and Pearce 1998; Pearce et al. 2000). Whole-rock major element compositions show that the Dazhuqu peridotites contain relatively higher Al_2O_3 (0.4–1.6 wt.%), CaO (0.50–1.9 wt.%) and lower MgO (41.8–45.5 wt.%) contents than the refractory IBM fore-arc mantle (these values are 0.12–1.04 wt.%, 0.30–2.36 wt.% and 42.4–50.0 wt.%, respectively) (Parkinson and Pearce 1998) (Table 2; Fig. 4a, b). These features confirm that the Dazhuqu samples are less refractory (i.e., lower degree of melting) than typical fore-arc peridotites.

The most significant chemical indicator for the high degree of melting of oceanic peridotites is high spinel Cr# value (Arai 1994; Dick and Bullen 1984; Hellebrand et al. 2001). Spinels with Cr# above 0.6 have been reported for modern fore-arc peridotites (Parkinson and Pearce 1998; Pearce et al. 2000) but very rarely for abyssal peridotites (Warren 2016). Therefore, Cr# values above 0.6 in spinels are widely considered as a chemical index for fore-arc peridotites. However, there are some cases where abyssal peridotites at modern MOR indeed contain spinels with Cr# > 0.6, such as the spinel peridotites from the Newfoundland margin drilled during ODP Leg 210 at Site 1277, North Atlantic Ocean (Müntener and Manatschal 2006) and some dunites and gabbro- and pyroxenite-veined peridotites from modern MOR (Warren 2016, as shown in Fig. 5b in this study). The spinels with Cr# above 0.6 of the Newfoundland case was interpreted as inheritance from ancient sub-arc mantle, which is consistent with the rifting processes forming the North Atlantic Ocean (Müntener and Manatschal 2006). However, the lack of extensional allochthons in the Yarlung Zangbo suture and regional areas (Gong et al. 2016) makes it a different case from the rifting-controlled OCT such as the Newfoundland–Iberia region. In contrast, the high-Cr# (> 0.6) spinels from the dunites and veined peridotites (Warren 2016) could be ascribed to a reactive origin, i.e., intense melt–rock interactions. It is well known that dunites and pyroxenite veins are formed by focused melt flow in the upper mantle (Büchl et al. 2002; Dick et al. 1984, 2010; Dygert et al. 2016; Kelemen and Dick 1995; Kelemen et al. 1995). Meanwhile, harzburgites can also be formed by melt percolation at a relatively small melt/rock ratio (Kelemen et al. 1992). As for the Dazhuqu mantle rocks in this study, the lherzolites have spinel Cr# that are less than 0.4, consistent with the compositions of residual abyssal peridotites (Fig. 5). It indicates that these lherzolites have experienced relatively low extents of melting typical of MOR environments. In contrast, the Dazhuqu harzburgites have spinel Cr# values overlapping with the ranges of both fore-arc and residual abyssal peridotites, with 2 (14DZQ78 and 14DZQ80) out of the 21 harzburgites containing spinel Cr# > 0.6 (Fig. 5). These two harzburgites are characterized by compositions indicative of intense melt–rock interactions, e.g., extremely elevated clinopyroxene LREE abundance (Fig. 7a), high clinopyroxene Ce and Sr contents (Fig. 7b) and $(Ce/Yb)_N$ (Fig. 10b) and $(Sm/Yb)_N$ (Fig. 11) ratios. They contain lowest clinopyroxene (0.7% and 1.5%, respectively) and highest olivine + orthopyroxene modal abundances among the Dazhuqu samples (Table 1), a composition that could be interpreted by the reactive scenario proposed by Kelemen et al. (1992) of dissolving clinopyroxene and producing olivine and orthopyroxene. In addition, the two samples also have spinel Cr# comparable to those of the dunites from the Luqu ophiolite (Fig. 5), which has been interpreted as the result of melt–rock interactions at high melt/rock ratios (Zhang et al. 2017). We argue that the high-Cr# signature of some Dazhuqu harzburgites is probably

derived from porous melt flow and melt–rock interaction, with lower melt/rock ratio with respect to the dunites and veined peridotites from modern MOR (Warren 2016). Thus, the extent of melting experienced by the Dazhuqu samples is comparable to that of the most depleted abyssal peridotites at modern MOR.

On the other hand, fluid fluxing increases the degree of melting in the mantle wedge, leaving peridotites that display strong depletion in their Ti concentrations (Bizimis et al. 2000). Hence, the extent and rate of depletion in clinopyroxene Ti content have been regarded as indicators for distinguishing hydrous melting in an arc setting from dry melting beneath MOR (Bizimis et al. 2000). Comparing the dry and hydrous melting results from Bizimis et al. (2000) (Fig. 13), the Dazhuqu peridotites have moderate clinopyroxene Ti contents that are comparable to the most depleted end of abyssal peridotites (Warren 2016). Most of the Dazhuqu samples deviate from the modeled dry melting trend (Bizimis et al. 2000) but show enrichments in Zr content of clinopyroxenes (Fig. 13) that could be ascribed to intense melt–rock interaction, as has been proposed for abyssal peridotites (Brunelli et al. 2006). These trace element features diverge significantly from the modeled refertilization–hydrous melting trend, which characterizes SSZ peridotites (Fig. 13; Bizimis et al. 2000).

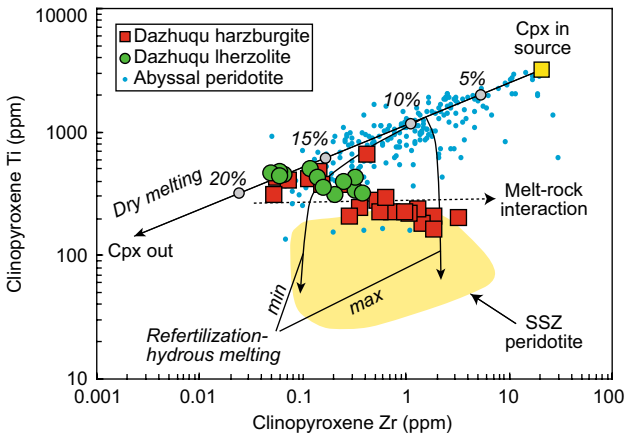

Fig. 13 Clinopyroxene Ti versus Zr of the Dazhuqu mantle peridotites. Data of abyssal peridotite are after the review in Warren (2016). Field of SSZ peridotite and melting trend are from Bizimis et al. (2000). Detailed parameters for melting modeling used by Bizimis et al. (2000) are listed in Appendix I. The boundaries of refertilization–hydrous melting model (Bizimis et al. 2000) are the limits of clinopyroxene compositions using the minimum (min) and maximum (max) concentrations in the fluid component, respectively. The minimum fluid components of Ti and Zr are 0 ppm and 16 ppm respectively, while the maximum fluid components of these elements are 436 ppm and 365 ppm, respectively. The melt–rock interaction trend (dashed line) are based on trajectories of the Dazhuqu harzburgite samples from this study and refertilization modeling results from Brunelli et al. (2006) (Appendix I)

The Dazhuqu peridotites show U-shaped whole-rock REE patterns (Fig. 7a), which were interpreted in previous studies (e.g., Xia et al. 2003) as a result of interaction between peridotites and boninitic melts. Similar arguments have also been proposed in studies of other ophiolite massifs along the YZSZ (e.g., Dai et al. 2011, 2013; Dubois-Côté et al. 2005; Xiong et al. 2017; Zhou et al. 2005). Boninite is commonly characterized by LREE enrichment relative to MREE and HREE and is traditionally taken as an indicator for a fore-arc setting (Crawford et al. 1989 and references therein). However, boninite is not the only candidate for the U-shaped REE patterns in the Yarlung Zangbo ophiolitic peridotites, because most (non-MORB) melts with which peridotites could interact are likely to have elevated LREE/HREE, such as OIB (ocean island basalt). In addition, abyssal peridotites at present-day MOR may also display LREE-enriched patterns in their whole-rock compositions (e.g., Day et al. 2017), demonstrating that the participation of boninitic magmas is not always required to produce such patterns. In this respect, it is misleading to attribute the U-shaped whole-rock REE patterns of the Dazhuqu peridotites to interaction with boninitic melts in a fore-arc setting.

Garnet-facies melting experienced by the Dazhuqu samples provides potential information to distinguish the Dazhuqu peridotites from fore-arc peridotites. About half of abyssal peridotite samples [data from Hellebrand et al. (2002)] show relatively low $(Sm/Yb)_N$ ratios at a given Yb_N in clinopyroxene, indicating garnet-facies melting (Fig. 11). In contrast, fore-arc peridotites, exemplified by the IBM mantle peridotites (Parkinson and Pearce 1998), commonly have much higher $(Sm/Yb)_N$ ratios at a given Yb_N in clinopyroxenes (Fig. 11). Only a few samples of the IBM system display weak depletion (< 3% partial melting) in the garnet stability field; most of the IBM samples have experienced solely spinel-facies partial melting. This distinction of the Dazhuqu and abyssal peridotites relative to the IBM samples might be associated with the depth where initial melting occurs. The Dazhuqu peridotites must have been derived from a depth that is not shallower than the spinel–garnet transition zone (about 85 km in depth; Robinson and Wood 1998). In contrast, fore-arc mantle is typically derived from a shallower depth (commonly < 80 km; Chen et al. 2018), inconsistent with the data from Dazhuqu mantle peridotites.

Most Dazhuqu lherzolites and harzburgites display relatively flat HSE patterns, though some harzburgite samples show variable PPGE and Re depletions because of high degrees of partial melting (Fig. 8). The HSE patterns and abundances of the Dazhuqu mantle peridotites are consistent with those of the most depleted end of abyssal peridotites. In this light, the Dazhuqu mantle rocks, particularly harzburgites, are equivalent in composition to the southern massifs (including Semail and Wadi Tayin) of the Oman ophiolite (Fig. 8), which are

interpreted as residues of partial melting as depleted as the most depleted abyssal peridotites beneath a paleo-MOR (Hanghøj et al. 2010). This is exemplified by their relatively refractory whole-rock compositions (Fig. 4), high spinel Cr# values (Fig. 5) and extremely low clinopyroxene Na_2O and Yb contents (Figs. 6, 10a). It should be noted that the mantle peridotites from the YZSZ (including Dazhuqu), along with the southern Oman massifs and most abyssal peridotites, show unfractionated Pt–Pd patterns, though a few of them are modified by Pd-rich sulfide melt–rock interactions (Fig. 8). This feature is fundamentally different from the fractionated Pt–Pd of some sub-arc mantle (e.g., mantle wedge xenoliths). For example, some mantle wedge xenoliths from the Kamchatka and Tabar–Lihir–Tanga–Feni (TLTF) arcs have extremely high Pt/Pd ratios (up to 126; Fig. 12d), which have been ascribed to multi-stage hydrous melting followed by the formation of Pt–Fe alloys typical of subduction zones (Kepezhinskas and Defant 2001; McInnes et al. 1999). In this light, the Dazhuqu mantle peridotites are different than the sub-arc mantle. A sub-arc mantle could experience an extremely high extent of melting because of the addition of subducted slab-derived H_2O-bearing fluids. In contrast, at a "dry" MOR environment, mantle rocks have commonly experienced a relatively lower extent of melting and hence do not show highly elevated Pt/Pd ratios. Similarly, the extent of melting experienced by the Dazhuqu mantle peridotites in this study must be lower than that of the Kamchatka and TLTF mantle wedge xenoliths with high Pt/Pd ratios. Therefore, we argue that the Dazhuqu samples are more similar to abyssal peridotites in their HSE pattern and abundance, other than typical sub-arc mantle, though the Pt–Pd indicator must be critically used.

Current knowledge has shown that it is hard to identify unequivocal chemical indicators distinguishing sub-oceanic mantle from its sub-continental and sub-arc counterparts (Rampone and Hofmann 2012). As for the Dazhuqu mantle peridotites from this study, their spinel compositions overlap with both fore-arc and abyssal peridotites; in addition, their Os isotopic ratios are also within the range of both abyssal peridotites and non-cratonic SCLM. Nonetheless, garnet-facies initial melting, abyssal peridotite-like HSE pattern and abundance and the lack of a correlation between Os isotopic ratio and some chemical fertility indexes positively suggest a sub-oceanic affinity for these rocks, rather than SCLM or sub-arc mantle. The Dazhuqu lherzolites and harzburgites show compositions that are similar to typical and most depleted abyssal peridotites, respectively. It implies their variable degrees of partial melting, which in turn could be as high as the extent of melting experienced by fore-arc mantle.

Broader implications for tectonic evolution of the Neo-Tethys Ocean

Ophiolites were widely interpreted, in early studies, as fossil oceanic lithosphere formed beneath MOR that were later emplaced onto continents (Gass 1968; Moores and Vine 1971; Nicolas et al. 1981). However, based on the arc-like geochemistry of associated crustal rocks, it has been argued that many ophiolites may have been generated in a SSZ setting (Alabaster et al. 1982; Miyashiro 1973; Pearce et al. 1984; Pearce and Robinson 2010; Whattam and Stern 2011). A SSZ origin has also been extensively proposed for the Yarlung Zangbo ophiolites (Dai et al. 2013; Dubois-Côté et al. 2005; Dupuis et al. 2005a; Hébert et al. 2012; Malpas et al. 2003; Xia et al. 2003; Xiong et al. 2016, 2017). Dai et al. (2013) and Xiong et al. (2016) argued that the Yarlung Zangbo ophiolites formed in a fore-arc basin above the subducted Neo-Tethys Ocean. They also proposed that the Cretaceous (120–130 Ma) crustal rocks in the ophiolites were accreted during fore-arc spreading and that the immense Neo-Tethyan oceanic lithosphere was subducted beneath the Asian continent (Dai et al. 2013). Hence, the only relicts of the Neo-Tethyan oceanic lithosphere are mafic rocks with OIB-type geochemistry found as blocks in the mélange to south of the ophiolites (Aitchison et al. 2000; An et al. 2017; Cai et al. 2012; Dupuis et al. 2005b, 2006; Searle et al. 1987; Ziabrev et al. 2004). Our study, however, suggests that the Dazhuqu mantle peridotites most probably formed as sub-oceanic mantle beneath the Neo-Tethyan MOR. They are unlikely to represent juvenile fore-arc mantle formed following subduction initiation (Whattam and Stern 2011). On the contrary, they were trapped, as an exotic block, at the southern margin of the Lhasa terrane (the Asian continent) in the Lower Cretaceous (~ 124 Ma; Liu et al. 2016) and became the basement for the fore-arc basin sedimentary rocks deposited soon afterwards (~ 119 Ma; Wang et al. 2017). Therefore, the Yarlung Zangbo ophiolites, particularly some massifs in the middle part (e.g., Dazhuqu), comprise an important component of the Neo-Tethyan oceanic lithosphere. The preservation of Neo-Tethyan sub-oceanic mantle along suture zones is not uncommon, as has been also proposed for the Oman ophiolite. However, its mechanism is still poorly constrained. Nicolas and Boudier (2017) proposed ridge–trench collision for the emplacement of the Oman ophiolite, which is probably plausible for the preservation of paleo-MOR oceanic lithospheres on land. This in turn underscores the need for a universal test of this mechanism along the Neo-Tethyan ophiolites in the near future.

Concluding remarks

We highlighted in this study some chemical indicators for the nature of the Dazhuqu mantle rocks in Tibet. (1) The derivation depth of initial melting and CI chondrite-normalized Pt–Pd (i.e., PPGE) pattern were used to distinguish sub-oceanic mantle from sub-arc mantle, because the former could be derived from the garnet stability field and has commonly experienced relatively lower extent of melting with respect to the latter. (2) The Na_2O of clinopyroxene and Al–Fe of spinel and the association between Os isotopic composition and some chemical fertility indexes were used to distinguish sub-oceanic mantle from non-cratonic SCLM.

The Dazhuqu mantle peridotites in this study are more similar to sub-oceanic mantle other than sub-arc or sub-continental mantle. We argue that the Dazhuqu mantle rocks most likely represent "fossil" abyssal peridotites formed beneath the Neo-Tethyan mid-ocean ridge. This directly implies an efficient preservation of the Neo-Tethyan sub-oceanic mantle along the Yarlung Zangbo suture zone, which in this light has a similar scenario to the Oman ophiolite.

Acknowledgements We thank Hong-Yue Wang, Ding-Shuai Xue and Yan-Hong Liu for their help in whole-rock major element analysis, Di Zhang for assistance with EPMA, and Yue-Heng Yang and Zhu-Yin Chu for help in mineral trace element, Re-Os isotope and HSE content analyses. We are grateful to Editor in Chief Othmar Müntener for editorial handling and helpful comments and to David van Acken and an anonymous reviewer for constructive comments and suggestions. Comments from Laurie Reisberg also improved the quality of an early version of the manuscript. This study was financially supported by the National Natural Science Foundation of China (grants 41673038, 41521062), the Key Research Program of Frontier Sciences from CAS (QYZDB-SSW-DQC032) and the Open Fund Project of State Key Laboratory of Lithospheric Evolution (201707).

References

Aitchison JC, Davis AM, Liu JB, Luo H, Malpas JG, McDermid IR, Wu HY, Ziabrev SV, Zhou MF (2000) Remnants of a Cretaceous intra-oceanic subduction system within the Yarlung–Zangbo suture (southern Tibet). Earth Planet Sci Lett183:231–244

Alabaster T, Pearce JA, Malpas J (1982) The volcanic stratigraphy and petrogenesis of the Oman ophiolite complex. Contrib Miner Petrol 82:168–183

Alard O, Luguet A, Pearson NJ, Griffin WL, Lorand J-P, Gannoun A, Burton KW, O'Reilly SY (2005) In situ Os isotopes in abyssal peridotites bridge the isotopic gap between MORBs and their source mantle. Nat 436:1005–1008

An W, Hu XM, Garzanti E (2017) Sandstone provenance and tectonic evolution of the Xiukang Mélange from Neotethyan subduction to India-Asia collision (Yarlung–Zangbo struture, south Tibet). Gondwana Res 41:222–234

Anders E, Grevesse N (1989) Abundances of the elements: Meteoritic and solar. Geochim Cosmochim Acta 53:197–214

Arai S (1994) Characterization of spinel peridotites by olivine-spinel compositional relationships: review and interpretation. Chem Geol 113:191–204

Bao PS, Su L, Wang J, Zhai QG (2013) Study on the tectonic setting for the ophiolites in xigaze, tibet. Acta Geol Sin 87:395–425

Becker H, Horan MF, Walker RJ, Gao S, Lorand J-P, Rudnick RL (2006) Highly siderophile element composition of the Earth's primitive upper mantle: Constraints from new data on peridotite massifs and xenoliths. Geochim Cosmochim Acta 70:4528–4550

Birck JL, Roy-Barman M, Capmas F (1997) Re–Os isotopic measurements at the femtomole level in natural samples. Geostand Newslet J Geostand Geoanal 21:19–27

Bizimis M, Salters VJM, Bonatti E (2000) Trace and REE content of clinopyroxenes from supra-subduction zone peridotites. Implications for melting and enrichment processes in island arcs. Chem Geol 165:67–85

Bizimis M, Griselin M, Lassiter JC, Salters VJM, Sen G (2007) Ancient recycled mantle lithosphere in the Hawaiian plume: Osmium–Hafnium isotopic evidence from peridotite mantle xenoliths. Earth Planet Sci Lett 257:259–273

Boillot G, Féraud G, Recq M, Girardeau J (1989) Undercrusting by serpentinite beneath rifted margins. Nature 341(6242):523–525

Bonatti E (1990) Subcontinental mantle exposed in the Atlantic Ocean on St Peter-Paul islets. Nature 345:800–802

Bonatti E, Ottonello G, Hamlyn PR (1986) Peridotites from the Island of Zabargad (St. John), Red Sea: petrology and geochemistry. J Geophys Res 91:599–631

Brandon AD, Snow JE, Walker RJ, Morgan JW, Mock TD (2000) 190Pt–186Os and 187Re–187Os systematics of abyssal peridotites. Earth Planet Sci Lett 177:319–335

Brenan JM, Bennett NR, Zajacz Z (2016) Experimental results on fractionation of the highly siderophile elements (HSE) at variable pressures and temperatures during planetary and magmatic differentiation. Rev Mineral Geochem 81:1–87

Brey GP, Köhler T (1990) Geothermobarometry in Four-phase Lherzolites II. New thermobarometers, and practical assessment of existing thermobarometers. J Petrol 31:1353–1378

Brunelli D, Seyler M, Cipriani A, Ottolini L, Bonatti E (2006) Discontinuous melt extraction and weak refertilization of mantle peridotites at the Vema Lithospheric Section (Mid-Atlantic Ridge). J Petrol 47:745–771

Büchl A, Brügmann G, Batanova VG, Münker C, Hofmann AW (2002) Melt percolation monitored by Os isotopes and HSE abundances: a case study from the mantle section of the Troodos Ophiolite. Earth Planet Sci Lett 204:385–402

Cai FL, Ding L, Leary RJ, Wang HQ, Xu Q, Zhang LY, Yue YH (2012) Tectonostratigraphy and provenance of an accretionary complex within the Yarlung–Zangpo suture zone, southern Tibet: insights into subduction–accretion processes in the Neo-Tethys. Tectonophysics 574–575:181–192

Chen JB, Zeng ZG (2007) Metasomatism of the peridotites from southern Mariana fore-arc: Trace element characteristics of clinopyroxene and amphibole. Sci China Ser D Earth Sci 50:1005–1012

Chen Y, Huang F, Shi GH, Wu F-Y, Chen X, Jin QZ, Su B, Guo S, Sein K, Nyunt TT (2018) Magnesium isotope composition of subduction zone fluids as constrained by jadeitites from Myanmar. J Geophys Res Solid Earth 123:7566–7585

Chu ZY, Wu FY, Walker RJ, Rudnick RL, Pitcher L, Puchtel IS, Yang YH, Wilde SA (2009) Temporal evolution of the lithospheric mantle beneath the eastern North China Craton. J Petrol 50:1857–1898

Coltorti M, Bonadiman C, O'Reilly SY, Griffin WL, Pearson NJ (2010) Buoyant ancient continental mantle embedded in oceanic lithosphere (Sal Island, Cape Verde Archipelago). Lithos 120:223–233

Crawford AJ, Falloon TJ, Green DH (1989) Classification, petrogenesis and tectonic setting of boninites. In: Crawford AJ (ed) Boninite and related rocks. Unwin Hyman, London, pp 1–49 in

Dai JG, Wang CS, Hébert R, Santosh M, Li YL, Xu JY (2011) Petrology and geochemistry of peridotites in the Zhongba ophiolite, Yarlung Zangbo Suture Zone: implications for the early cretaceous intra-oceanic subduction zone within the Neo-Tethys. Chem Geol 288:133–148

Dai JG, Wang CS, Polat A, Santosh M, Li YL, Ge YK (2013) Rapid forearc spreading between 130 and 120 Ma: evidence from geochronology and geochemistry of the Xigaze ophiolite, southern Tibet. Lithos 172–173:1–16

Day JMD, Walker RJ, Warren JM (2017) 186Os–187Os and highly siderophile element abundance systematics of the mantle revealed by abyssal peridotites and Os-rich alloys. Geochimica et Cosmochimica Acta 200:232–254

Dewey JF, Shackleton RM, Chang CF, Sun YY (1988) The tectonic evolution of the Tibetan Plateau. Philos Trans R Soc Lond Ser A Math Phys Sci 327:379–413

Dick HJB, Bullen T (1984) Chromian spinel as a petrogenetic indicator in abyssal and alpine-type peridotites and spatially associated lavas. Contrib Miner Petrol 86:54–76

Dick HJB, Fisher RL, Bryan WD (1984) Mineralogic variability of the uppermost mantle along mid-ocean ridges. Earth Planet Sci Lett 69:88–106

Dick HJB, Lissenberg CJ, Warren JM (2010) Mantle melting, melt-transport, and delivery beneath a slow-spreading ridge: the paleo-MAR from 23°15′N to 23°45′N. J Petrol 51:425–467

Dilek Y, Furnes H (2011) Ophiolite genesis and global tectonics: Geochemical and tectonic fingerprinting of ancient oceanic lithosphere. Geol Soc Am Bull 123:387–411

Dubois-Côté V, Hébert R, Dupuis C, Wang CS, Li YL, Dostal J (2005) Petrological and geochemical evidence for the origin of the Yarlung Zangbo ophiolites, southern Tibet. Chem Geol 214:265–286

Dupuis C, Hébert R, Dubois-Côté V, Guilmette C, Wang CS, Li YL, Li ZJ (2005a) The Yarlung Zangbo Suture Zone ophiolitic mélange (southern Tibet): new insights from geochemistry of ultramafic rocks. J Asian Earth Sci 25:937–960

Dupuis C, Hébert R, Dubois-Côté V, Wang CS, Li ZJ (2005b) Petrology and geochemistry of mafic rocks from mélange and flysch units adjacent to the Yarlung Zangbo Suture Zone, southern Tibet. Chem Geol 214:287–308

Dupuis C, Hébert R, Dubois-Côté V, Guilmette C, Wang CS, Li ZJ (2006) Geochemistry of sedimentary rocks from mélange and flysch units south of the Yarlung Zangbo suture zone, southern Tibet. J Asian Earth Sci 26:489–508

Dygert N, Liang Y, Kelemen PB (2016) Formation of plagioclase lherzolite and associated dunite–harzburgite–lherzolite sequences by multiple episodes of melt percolation and melt–rock reaction: an example from the Trinity Ophiolite, California, USA. J Petrol 57:815–838

Gass IG (1968) Is the Troodos massif of Cyprus a fragment of Mesozoic ocean floor? Nature 220:39–42

Gehrels G, Kapp P, DeCelles P, Pullen A, Blakey R, Weislogel A, Ding L, Guynn J, Martin A, McQuarrie N, Yin A (2011) Detrital zircon geochronology of pre–Tertiary strata in the Tibetan–Himalayan orogen. Tectonics 30:TC5016. https://doi.org/10.1029/2011TC002868

Girardeau J, Mercier JCC, Cao YG (1985a) Origin of the xigaze ophiolite, yarlung zangbo suture zone, southern tibet. Tectonophysics 119:407–433

Girardeau J, Mercier JCC, Wang XB (1985b) Petrology of the mafic rocks of the Xigaze ophiolite, Tibet: implications for the genesis of the oceanic lithosphere. Contrib Miner Petrol 90:309–321

Gong XH, Shi RD, Griffin WL, Huang QS, Xiong Q, Chen SS, Zhang M, O'Reilly SY (2016) Recycling of ancient subduction-modified mantle domains in the Purang ophiolite (southwestern Tibet). Lithos 262:11–26

Griffin WL, Powell WJ, Pearson NJ, O'Reilly SY (2008) GLITTER: data reduction software for laser ablation ICP-MS. In: Sylvester P (ed) Laser Ablation-ICP-MS in the earth sciences: current practices and outstanding issues, Mineralogical Association of Canada Short Course Series, vol 40, pp 307–311

Griffin WL, Afonso JC, Belousova EA, Gain SE, Gong XH, González-Jiménez JM, Howell D, Huang JX, McGowan N, Pearson NJ, Satsukawa T, Shi R, Williams P, Xiong Q, Yang JS, Zhang M, O'Reilly SY (2016) Mantle recycling: transition zone metamorphism of Tibetan ophiolitic peridotites and its tectonic implications. J Petrol 57:655–684

Hanghøj K, Kelemen PB, Hassler D, Godard M (2010) Composition and genesis of depleted mantle peridotites from the waditayin massif, oman ophiolite; major and trace element geochemistry, and Os isotope and PGE systematics. J Petrol 51:201–227

Harvey J, Gannoun A, Burton KW, Rogers NW, Alard O, Parkinson IJ (2006) Ancient melt extraction from the oceanic upper mantle revealed by Re-Os isotopes in abyssal peridotites from the Mid-Atlantic ridge. Earth Planet Sci Lett 244:606–621

Hébert R, Bezard R, Guilmette C, Dostal J, Wang CS, Liu ZF (2012) The Indus-Yarlung Zangbo ophiolites from Nanga Parbat to Namche Barwa syntaxes, southern Tibet: first synthesis of petrology, geochemistry, and geochronology with incidences on geodynamic reconstructions of Neo-Tethys. Gondwana Res 22:377–397

Hellebrand E, Snow JE (2003) Deep melting and sodic metasomatism underneath the highly oblique-spreading Lena Trough (Arctic Ocean). Earth Planetary Science Letters 216:283–299

Hellebrand E, Snow JE, Dick HJB, Hofmann AW (2001) Coupled major and trace elements as indicators of the extent of melting in mid-ocean-ridge peridotites. Nature 410:677–681

Hellebrand E, Snow JE, Hoppe P, Hofmann AW (2002) Garnet-field melting and late stage refertilization in 'residual' abyssal peridotites from the Central Indian Ridge. J Petrol 43:2305–2338

Horan MF, Walker RJ, Morgan JW, Grossman JN, Rubin AE (2003) Highly siderophile elements in chondrites. Chem Geol 196:5–20

Johnson KTM, Dick HJB, Shimizu N (1990) Melting in the oceanic upper mantle: an ion microprobe study of diopsides in abyssal peridotites. J Geophys Res 95:2661–2678

Keays RR (1995) The role of komatiitic and picritic magmatism and S-saturation in the formation of ore deposits. Lithos 34:1–18

Kelemen PB, Dick HJB (1995) Focused melt flow and localized deformation in the upper mantle: Juxtaposition of replacive dunite and ductile shear zones in the Josephine peridotite, SW Oregon. J Geophys Res Solid Earth 100(B1):423–438

Kelemen PB, Dick HJB, Quick JE (1992) Formation of harzburgites by pervasive melt/rock reaction in the upper mantle. Nature 358:635–641

Kelemen PB, Shimizu N, Salters VJM (1995) Extraction of mid-ocean-ridge basalt from the upwelling mantle by focused flow of melt in dunite channels. Nature 375:747–753

Kepezhinskas P, Defant MJ (2001) Nonchondritic Pt/Pd ratios in arc mantle xenoliths: Evidence for platinum enrichment in depleted island-arc mantle sources. Geol 29:851–854

Lassiter JC, Byerly BL, Snow JE, Hellebrand E (2014) Constraints from Os-isotope variations on the origin of Lena Trough abyssal peridotites and implications for the composition and evolution of the depleted upper mantle. Earth Planet Sci Lett 403:178–187

Liu CZ, Snow JE, Hellebrand E, Brugmann G, von der Handt A, Büchl A, Hofmann AW (2008) Ancient, highly heterogeneous mantle beneath Gakkel ridge, Arctic Ocean. Nature 452:311–316

Liu CZ, Wu FY, Chu ZY, Ji WQ, Yu LJ, Li JL (2012) Preservation of ancient Os isotope signatures in the Yungbwa ophiolite

(southwestern Tibet) after subduction modification. J Asian Earth Sci 53:38–50

Liu T, Wu FY, Zhang LL, Zhai QG, Liu CZ, Ji WB, Zhang C, Xu Y (2016) Zircon U-Pb geochronological constraints on rapid exhumation of the mantle peridotite of the Xigaze ophiolite, southern Tibet. Chem Geol 443:67–86

Lorand J-P, Gros M, Pattou L (1999) Fractionation of platinum-group element in the upper mantle: a detailed study in Pyrenean orogenic peridotites. J Petrol 40:951–987

Lorand J-P, Alard O, Godard M (2009) Platinum-group element signature of the primitive mantle rejuvenated by melt-rock reactions: evidence from Sumail peridotites (Oman Ophiolite). Terra Nova 21:35–40

Luguet A, Reisberg L (2016) Highly siderophile element and 187Os signatures in non-cratonic basalt-hosted peridotite xenoliths: Unravelling the origin and evolution of the Post-Archean lithospheric mantle. Rev Mineral Geochem 81:305–367

Luguet A, Lorand J-P, Seyler M (2003) Sulfide petrology and highly siderophile element geochemistry of abyssal peridotites: A coupled study of samples from the Kane Fracture Zone (45°W 23°20N, MARK Area, Atlantic Ocean). Geochim Cosmochim Acta 67:1553–1570

Luguet A, Lorand J-P, Alard O, Cottin J-Y (2004) A multi-technique study of platinum group element systematic in some Ligurian ophiolitic peridotites, Italy. Chem Geol 208:175–194

Malpas J, Zhou MF, Robinson PT, Reynolds PH (2003) Geochemical and geochronological constraints on the origin and emplacement of the Yarlung Zangbo ophiolites, Southern Tibet. Geol Soc Lond Speicial Publ 218:191–206

McCarthy A, Müntener O (2015) Ancient depletion and mantle heterogeneity: Revisiting the Permian–Jurassic paradox of Alpine peridotites. Geology 43:255–258

McInnes BIA, McBride JS, Evans NJ, Lambert DD, Andrew AS (1999) Osmium isotope constraints on ore Metal recycling in subduction zones. Science 286:512–516

Meisel T, Moser J (2004) Reference materials for geochemical PGE analysis: new analytical data for Ru, Rh, Pd, Os, Ir, Pt and Re by isotope dilution ICP-MS in 11 geological reference materials. Chem Geol 208:319–338

Meisel T, Walker RJ, Irving AJ, Lorand JP (2001) Osmium isotopic compositions of mantle xenoliths: a global perspective. Geochim Cosmochim Acta 65:1311–1323

Metcalfe I (2006) Palaeozoic and Mesozoic tectonic evolution and palaeogeography of East Asian crustal fragments: the Korean Peninsula in context. Gondwana Res 9:24–46

Miyashiro A (1973) The Troodos ophiolitic complex was probably formed in an island arc. Earth Planet Sci Lett 19:218–224

Moores EM, Vine FJ (1971) The Troodos Massif, Cyprus and other ophiolites as oceanic crust: evolution and implications. Philos Trans R Soc Lond Ser A Math Phys Sci 268:443–466

Morgan JW (1986) Ultramafic xenoliths: clues to the Earth's late accretionary history. J Geophys Res Atmos 91:12375–12387

Müntener O, Manatschal G (2006) High degrees of melt extraction recorded by spinel harzburgite of the newfoundland margin: the role of inheritance and consequences for the evolution of the southern North Atlantic. Earth Planet Sci Lett 252:437–452

Müntener O, Manatschal G, Desmurs L, Pettke T (2010) Plagioclase peridotites in ocean–continent transitions: refertilized mantle domains generated by melt stagnation in the shallow mantle lithosphere. J Petrol 51:255–294

Nicolas A, Boudier F (2017) Emplacement of Semail–Emirates ophiolite at ridge–trench collision. Terra Nova 29:127–134

Nicolas A, Girardeau J, Marcoux J, Dupre B, Wang XB, Cao YG, Zheng HX, Xiao XC (1981) The xigaze ophiolite (Tibet): a peculiar oceanic lithosphere. Nature 294:414–417

Niu YL (1997) Mantle melting and melt extraction processes beneath ocean ridges: evidence from abyssal peridotites. J Petrol 38:1047–1074

Niu YL (2004) Bulk-rock major and trace element compositions of abyssal peridotites: implications for mantle melting, melt extraction and post-melting processes beneath mid-ocean ridges. J Petrol 45:2423–2458

Niu XL, Yang JS, Dilek Y, Xu JF, Li J, Chen SY, Feng GY, Liu F, Xiong FH, Liu Z (2015) Petrological and Os isotopic constraints on the origin of the Dongbo peridotite massif, Yarlung Zangbo Suture Zone, Western Tibet. J Asian Earth Sci 110:72–84

O'Reilly SY, Zhang M, Griffin WL, Begg G, Hronsky J (2009) Ultradeep continental roots and their oceanic remnants: a solution to the geochemical "mantle reservoir". problem? Lithos 211S:1043–1054

Pan GT, Wang LQ, Li RS, Yuan SH, Ji WH, Yin FG, Zhang WP, Wang BD (2012) Tectonic evolution of the Qinghai-Tibet Plateau. J Asian Earth Sci 53:3–14

Parkinson IJ, Pearce JA (1998) Peridotites from the Izu–Bonin–Mariana forearc (ODP Leg 125): evidence for mantle melting and melt-mantle interaction in a suprasubduction zone setting. J Petrol 39:1577–1618

Pearce JA, Robinson PT (2010) The Troodos ophiolitic complex probably formed in a subduction initiation, slab edge setting. Gondwana Res 18:60–81

Pearce JA, Lippard SJ, Roberts S (1984) Characteristics and tectonic significance of supra-subduction zone ophiolites. Geol Soc Lond Spec Publ 16:77–94

Pearce NJG, Perkins WT, Westgate JA, Gorton MP, Jackson SE, Neal CR, Chenery SP (1997) A compilation of new and published major and trace element data for NIST SRM610 and NIST SRM 612 glass reference materials. Geostand Newslett 20:247–261

Pearce JA, Baker PF, Edwards SJ, Parkinson IJ, Leat PT (2000) Geochemistry and tectonic significance of peridotites from the South Sandwich arc-basin system, South Atlantic. Contrib Miner Petrol 139:36–53

Pearson DG, Irvine GJ, Ionov DA, Boyd FR, Dreibus GE (2004) Re–Os isotope systematics and platinum group element fractionation during mantle melt extraction: a study of massif and xenolith peridotite suites. Chem Geol 208:29–59

Rampone E, Hofmann AW (2012) A global overview of isotopic heterogeneities in the oceanic mantle. Lithos 148:247–261

Rampone E, Hofmann AW, Piccardo GB, Vannucci R, Bottazzi P, Ottolini L (1995) Petrology, mineral and isotope geochemistry of the external liguride peridotites (Northern Apennines, Italy). J Petrol 36:81–105

Rampone E, Hofmann AW, Raczek I (1998) Isotopic contrasts within the Internal Liguride ophiolite (N Italy): the lack of a genetic mantle–crust link. Earth Planet Sci Lett 163:175–189

Rampone E, Piccarod G, Hofmann AW (2008) Multi-stage melt-rock interaction in the Mt Maggiore (Corsica, France) ophiolitic peridotites: microstructural and geochemical evidence. Contrib Miner Petrol 156:453–475

Reisberg L, Lorand JP (1995) Longevity of sub-continental mantle lithosphere from osmium isotope systematics in orogenic peridotite massifs. Nature 376:159–162

Robinson JAC, Wood BJ (1998) The depth of the spinel to garnet transition at the peridotite solidus. Earth Planet Sci Lett 164(1–2):277–284

Rudnick RL, Walker RJ (2009) Interpreting ages from Re–Os isotopes in peridotites. Lithos 112S:1083–1095

Searle MP, Windley BF, Coward MP, Cooper DJW, Rex AJ, Rex D, Li TD, Xiao XC, Jan MQ, Thakur VC, Kumar S (1987) The closing of Tethys and the tectonics of the Himalaya. Geol Soc Am Bull 98:678–701

Sengor AMC, Natalin BA (1996) Paleotectonics of Asia: fragments of a synthesis. In: Yin A, Harrison M (eds) The Tectonics of Asia. Cambridge University Press, New York, pp 486–640 in

Seyler M, Lorand J-P, Dick HJB, Drouin M (2007) Pervasive melt percolation reactions in ultra-depleted refractory harzburgites at the Mid-Atlantic Ridge, 15°20′N: ODP Hole 1274. Contrib Miner Petrol 153:303–319

Shirey SB, Walker RJ (1998) The Re–Os isotope system in cosmochemistry and high-temperature geochemistry. Annu Rev Earth Planet Sci 26:423–500

Snow JE, Reisberg L (1995) Os isotopic systematics of the MORB mantle: results from altered abyssal peridotites. Earth Planet Sci Lett 136:723–733

Snow JE, Schmidt G (1999) Proterozoic melting in the northern peridotite Massif, Zabargad Island: Os isotopic evidence. Terra Nova 11:45–50

Snow JE, Schmidt G, Rampone E (2000) Os isotopes and highly siderophile elements (HSE) in the Ligurian ophiolites, Italy. Earth Planet Sci Lett 175:119–132

Stracke A, Snow JE, Hellebrand E, von der Handt A, Bourdon B, Birdaum K, Günther D (2011) Abyssal peridotite Hf isotopes identify extreme mantle depletion. Earth Planet Sci Lett 308:359–368

Sun SS, McDonough W (1989) Chemical and isotopic systematics of oceanic basalts: implications for mantle composition and processes. Geol Soc Lond Spec Publ 42:313–345

Tribuzio R, Thirlwall MF, Vannucci R (2004) Origin of the gabbro-peridotite association from the Northern Apennine Ophiolites (Italy). J Petrol 45:1109–1124

van Acken D, Becker H, Walker RJ (2008) Refertilization of Jurassic oceanic peridotites from the Tethys Ocean—implications for the Re–Os systematics of the upper mantle. Earth Planet Sci Lett 268:171–181

van Acken D, Becker H, Hammerschmidt K, Walker RJ, Wombacher F (2010) Highly siderophile elements and Sr–Nd isotopes in refertilized mantle peridotites—a case study from the Totalp ultramafic body, Swiss Alps. Chem Geol 276:257–268

Walker RJ, McDonough WF, Honesto J, Chabot NL, McCoy TJ, Ash RD, Bellucci JJ (2008) Modeling fractional crystallization of group IVB iron meteorites. Geochim Cosmochim Acta 72:2198–2216

Wang XB, Bao PS, Deng WM, Wang FG (1987) Xizang (Tibet) Ophiolites. Geological Publishing House, Beijing. (In Chinese)

Wang JG, Hu XM, Garzanti E, An W, Liu XC (2017) The birth of the Xigaze forearc basin in southern Tibet. Earth Planet Sci Lett 465:38–47

Warren JM (2016) Global variations in abyssal peridotite compositions. Lithos 248–251:193–219

Warren JM, Shimizu N, Sakaguchi C, Dick HJB, Nakamura E (2009) An assessment of upper mantle heterogeneity based on abyssal peridotite isotopic compositions. J Geophys Res Solid Earth 114:B12203. https://doi.org/10.1029/2008JB006186

Whattam SA, Stern RJ (2011) The "subduction initiation rule": a key for linking ophiolites, intra-oceanic forearcs, and subduction initiation. Contrib Miner Petrol 162:1031–1045

Wilson JT (1968) Static or mobile earth: the current scientific revolution. Proc Am Philos Soc 112:309–320

Workman RK, Hart SR (2005) Major and trace element composition of the depleted MORB mantle (DMM). Earth Planet Sci Lett 231:53–72

Wu FY, Huang BC, Ye K, Fang AM (2008) Collapsed Himalayan-Tibetan orogen and the rising Tibetan Plateau. Acta Petrol Sinica 24:1–30 (In Chinese with English abstract)

Wu FY, Liu CZ, Zhang LL, Zhang C, Wang JG, Ji WQ, Liu XC (2014) Yarlung zangbo ophiolite: a critical updated view. Acta Petrol Sinica 30:293–325 (In Chinese with English abstract)

Xia B, Yu HX, Chen GW, Qi L, Zhao TP, Zhou MF (2003) Geochemistry and tectonic environment of the Dagzhuka ophiolite in the Yarlung-Zangbo suture zone, Tibet. Geochem J 37:311–324

Xiong Q, Griffin WL, Zheng JP, O'Reilly SY, Pearson NJ, Xu B, Belousova EA (2016) Southward trench migration at ~ 130–120 Ma caused accretion of the Neo-Tethyan forearc lithosphere in Tibetan ophiolites. Earth Planet Sci Lett 438:57–65

Xiong FH, Yang JS, Robinson PT, Gao J, Chen YH, Lai SM (2017) Petrology and geochemistry of peridotites and podiform chromitite in the Xigaze ophiolite, Tibet: Implications for a suprasubduction zone origin. J Asian Earth Sci 146:56–75

Yin A, Harrison TM (2000) Geologic evolution of the Himalayan-Tibetan orogen. Annu Rev Earth Planet Sci 28:211–280

Zhang C, Liu CZ, Wu FY, Ji WB, Liu T, Xu Y (2017) Ultra-refractory mantle domains in the Luqu ophiolite (Tibet): petrology and tectonic setting. Lithos 286–287:252–263

Zhou MF, Robinson PT, Malpas J, Edwards SJ, Qi L (2005) REE and PGE geochemical constraints on the formation of dunites in the luobusa ophiolite, Southern Tibet. J Petrol 46:615–639

Zhu DC, Zhao ZD, Niu Y, Dilek Y, Hou ZQ, Mo XX (2013) The origin and pre-Cenozoic evolution of the Tibetan Plateau. Gondwana Res 23:1429–1454

Ziabrev SV, Aitchison JC, Abrajevitch AV, Badengzhu Davis AM, Luo H (2003) Precise radiolarian age constraints on the timing of ophiolite generation and sedimentation in the Dazhuqu terrane, Yarlung–Tsangpo suture zone, Tibet. J Geol Soc Lond 160:591–599

Ziabrev SV, Aitchison JC, Abrajevitch AV, Badengzhu Davis AM, Luo H (2004) Bainang Terrane, Yarlung–Tsangpo struture, southern Tibet (Xizang, China): a record of intra-Neotethyan subduction–accretion processes preserved on the roof of the world. J Geol Soc Lond 161:523–538